REPORT DOCUMENTATION PAGE

Form Approved
OMB NO. 0704-0188

1.REPORT DATE (MM-DD-YYYY)	2.REPORT TYPE	3. DATES COVERED
01/05/2007	FINAL	10/01/2004 - 12/31/2006

4. TITLE AND SUBTITLE
Predictive Computations of Properties of Wide-Gap and Nano-Semiconductors

5a. CONTRACT NUMBER

5b. GRANT NUMBER
N00014-05-1-0009

5c. PROGRAM ELEMENT NUMBER

6. AUTHOR (S)
DIOLA BAGAYOKO, PH.D., PROJECT DIRECTOR
G. L. ZHAO, PH.D., CO-PRINCIPAL INVESTIGATOR

5d. PROJECT NUMBER

5e. TASK NUMBER

5f. WORK UNIT NUMBER

7. PERFORMING ORGANIZATION NAME (S) AND ADDRESS (ES)
Southern University and A & M College, Office of Research, 500 Harding Boulevard, Baton Rouge, LA 70813

8. PERFORMING ORGANIZATION REPORT NUMBER

9. SPONSORING/MENTORING AGENCY NAME (S) AND ADDRESS (ES)
Colin Wood, DSc, Ph.D., Code 312, Office of Naval Research (ONR) Room 9-06, 1 Liberty Center, 875 N. Randolph St., Arlington VA 22203

10.SPONSOR/MONITOR'S ACRONYM (S)
ONR

11.SPONSOR/MONITOR'S REPORT NUMBER (S)

12. DISTRIBUTION/AVAILABILITY STATEMENT
UNLIMITED

DISTRIBUTION STATEMENT A
Approved for Public Release
Distribution Unlimited

13. SUPPLEMENTARY NOTES

14. ABSTRACT
We report the progress made in the implementation of the aforementioned project. To date, we have strictly adhered to the provisions in the proposal relative to the research personnel, materials under study (i.e., GaN, InN, ZnO, Carbon Nanotubes), and the overall research tasks (i.e., computations and theoretical analysis). We have consequently generated new knowledge that is reported in several articles. Twelve (12) articles have already been published, including six (6) in refereed journals and four (4) in refereed conference proceedings. These articles are appended to this report. We have made fourteen (14) technical presentations on our findings, including at two (3) national and two (2) international conferences. The utter significance of our findings resides in the fact that they have confirmed our resolution of a long-standing problem in materials science stemming from a 30 to 50% or more underestimation, by theory, of the measured energy gaps (atoms, molecules, and clusters) and band gaps (semiconductors and insulators). Specifically, density functional theory (DFT) and its local density approximation (LDA) had been blamed, before our work, for the resulting gross disagreements between theory and experiment. Unlike previous works, we have obtained the experimentally measured band gaps of wurtzite InN, ZnO, and of several single walled carbon nanotubes. This feat was accomplished by our utilization of the Bagayoko, Zhao, and Williams (BZW) method. Further, we have predicted the band gap of cubic InN for which no experimental results are available. It is befitting that this ONR funded project exonerated DFT and LDA that were obtained by a project funded by ONR and for which Dr. Walter Kohn received the 1998 Nobel Prize in Chemistry. *With the BZW method, DFT and LDA calculations can now predict the energy or band gaps of materials, from atoms and molecules to semiconductors and insulators.* The importance of this point cannot be overemphasized in light of the currency of nanoscience and technology: indeed, at the nanoscale, accurately calculated energy or band gaps are indispensable in informing and in guiding device design and fabrication. Incidentally, the above feat of the BZW method should apply to nuclei in the shell model!

15. SUBJECT TERMS: DENSITY FUNCTIONAL THEORY; LOCAL DENSITY APPROXIMATION; BAGAYOKO, ZHAO, AND WILLIAMS (BZW) METHOD; PREDICTION OF ELECTRONIC PROPERTIES, INCLUDING ENERGY OR BAND GAPS; RAYLEIGHT-RITZ VARIATIONAL METHOD; LINEAR COMBINATION OF ATOMIC ORBITAL (LCAO).

16. SECURITY CLASSIFICATION OF:			17. LIMITATION OF ABSTRACT	18.NUMBER OF PAGES	19a. NAME OF RESPONSIBLE PERSON
UNCLASSIFIED					DIOLA BAGAYOKO, PH.D.
a. REPORT	b. ABSTRACT	c. THIS PAGE	UU	40	19b. TELEPHONE NUMBER (Include area code) (225) 771-2730

FINAL REPORT

GRANT#: N00014-05-1-0009

PRINCIPAL INVESTIGATORS: Diola Bagayoko, Ph.D., Southern University System Distinguished Professor of Physics, Project Director, and G. L. Zhao, Ph.D., Associate Professor of Physics, SUBR, Co-Principal Investigator

Program Officer, Office of Naval Research (ONR): Colin Wood, DSc, Ph.D., Code 312, Office of Naval Research (ONR), Room 9-06, 1 Liberty Center, 875 N. Randolph St., Arlington VA 22203. Telephone: (703) 696-4218.

INSTITUTION: Southern University and A & M College in Baton Rouge (SUBR)

GRANT TITLE: Predictive Computations of Properties of Wide-Gap and Nano-Semiconductors

AWARD PERIOD: October 1, 2004 to December 31, 2006

OBJECTIVE: As per the initial proposal, the aim of this project is (a) to produce new scientific knowledge on wide-gap and nano-semiconductors, with specific materials including GaN, InN, AlN, and carbon nanotubes, (b) to develop analytical and computational techniques and computer codes for wider applications in descriptive and predictive investigations of the above materials and others, and (c) to provide research training for undergraduate and graduate students, including minority students at SUBR.

APPROACH: Our *technical approach or method*, as per the proposal, consists of the following. Like most previous calculations of electronic and related properties of semiconductors, we employ a density functional theory (DFT) potential. This potential is often selected, by design, from the local density approximation (LDA) to the general DFT. We also utilize, like previous works, the linear combination of atomic orbital (LCAO) formalism in a Rayleigh-Ritz variational procedure to perform self-consistent calculations. Our calculations, to date, are for zero temperature and are non-relativistic.

The key distinction between our method and those of all previous calculations by other groups resides in our adherence to the Bagayoko, Zhao, and Williams (BZW) method in the implementation of the LCAO formalism. References clearly identified in the attached articles fully describe this method. *Essentially, this method resolved the long-standing underestimation, by theory (by 30 to 50% or more), of measured energy or band gaps of finite (atoms, clusters, molecules) and infinite (semiconductors insulators) systems*. As explained in the attached articles and references therein, BZW first identified a basis set and variational effect that is responsible for an unphysical lowering of the low-lying, unoccupied energy levels or bands of materials. This unphysical lowering is shown to be a mathematical artifact stemming from the Rayleigh theorem. BZW subsequently introduced a rigorous method of performing variational calculations in such a way that the above unphysical lowering of unoccupied levels or bands is

totally avoided. *Let us underscore that the underestimation of energy and band gaps is a trivial consequence of the above unphysical lowering of unoccupied levels of bands.*

The BZW method generally entails the performance of three (3) or more self-consistent calculations. The first calculation employs the minimal basis set for the system and progressively augment it in subsequent calculations. The **occupied** energy levels or bands of a calculation the next, consecutive calculation whose basis set is larger. As explained in detail in the articles, successive calculations have different basis sets: the basis set for the latter is obtained by augmenting that of the former with the next excited state orbital an atomic or ionic species that is present in the system under study (i.e., In and N for InN). This process continues until the occupied energies are found to be identical for two consecutive calculation N and (N+1). Then, the results of calculation N are the physical ones for the system under study (and not those of calculation N+1). This criterion for stopping the process rests trivially on the facts that (a) density functional theory is a ground state theory and (b) only the wave functions of the occupied states are including in the construction and reconstruction of the charge density (and hence the potential and the Hamiltonian) in the self-consistency process.

Once the correct energy levels or bands are obtained, then we proceed to calculate a host of properties that include the energy or band gaps, optical transition energies, the total energy, the total and partial densities of states, the effective masses of charge carriers (for application in transport studies), and the optical properties (i.e., the complex dielectric functions). Of course, the total energy curves are utilized to compute the bulk modulus.

PROJECT MANAGEMENT AND OVERSIGHT : In addition to the above *technical approach*, we should note that our *programmatic implementation* also adhered to the proposal. In particular, we have hired Dr. Hua Jin as the Postdoctoral Associate. She has been performing excellently, not only in carrying out research tasks, but also in assisting the investigators in their training of students on the complex software package utilized in this work. A graduate and undergraduate students, mostly African American, have also been employed. SUBR is a Historically Black College and University (HBCU). The effort levels of the investigators (D. Bagayoko and G. L. Zhao) are as per the proposal.

We timely submitted a progress report in 2005, following the instructions in the Award Letter, These instructions included an address for the Technical Monitor, Dr. Colin Wood. While the various copies of the report were received by the concerned ONR officials, the one to the Technical Monitor was not delivered and we did not know this fact until around the end of the summer of 2006. [The address in the Award Letter is totally different from the one Dr. Wood provided to us at the end of the summer of 2005.] We then sent the complete report to Dr. Colin Wood as an email attachment (PDF). The second year funding we were supposed to receive in the fall of 2005 was not received until the end of the summer of 2006, a month or so from the initial expiration date of the project (in September 2006). We wrote to request a no-cost extension for one year. At the recommendation of Dr. Wood, we received six month extension so that the actual expiration date of the project is December 31, 2006. This situation led to serious strains in the final phase of the project where much work had to be done within approximately four (4) months as opposed to close to a year. We managed, in addition to Dr. H. Jin, to hire Ms. L. Franklin (who co-authored 2 of the attached refereed articles), and Dr. Yang for a few months. In so doing, we completed the work. We could not, however, hire a graduate student for half a year (with no support in the spring of 2007). Hence, the $12,000 or so of graduate assistantship,

with the associated overhead, will be returned to ONR. The circumstances above, we hope, show that these residuals were not due to our failure to manage the project very well.

ACCOMPLISHMENTS: As summarized in the abstract of this report, we have published twelve (12) articles, made fourteen (14) technical presentations, three of which were at international conferences. To reduce redundancy, we refer the reader to the following full listing of the articles, with referencing information. We also list the presentations below. The subtitles below, for accomplishments, are keyed to the objectives enunciated above.

Publications (12)

"Structural, Elastic, and Electronic Properties of Deformed Carbon Nanotubes under Uniaxial Strain." A. Pullen, G. L. Zhao, D. Bagayoko, and L. Yang. Physical Review B 71, 205410.

"Ab-initio Simulations of the Growth and Structural Properties of Short Carbon Nanobells." G. L. Zhao, D. Bagayoko, and E. G. Wang. Accepted for publication in the Proceedings of the 2005 China Conference on Nanoscience and Technology, Beijing, China, July 2005.

"A Universal Relation Between the Densities of States Near van Hove Singularities and the Effective Electron Masses in 1-Dimensional Semiconductors." G. L. Zhao and D. Bagayoko. Accepted for publication in the Proceedings of the 2005 China Conference on Nano-Science and Technology , Beijing, China, July 2005.

"LDA and LCAO-BZW Description of Electronic Properties of Wurtzite Zinc Oxide (w-ZnO)." Diola Bagayoko, Lashounda Franklin, and G. L. Zhao, accepted for publications in Proceedings of the 2005 National Conference of the National Society of Black Physicists (www.nsbp.org), Orlando, Florida.

"Predictions of Electronic, Structural, and Elastic Properties of Cubic InN." Diola Bagayoko, Lashounda Franklin, and G. L. Zhao, Journal of Applied Physics 96, 4297-4301, 2004.

"Density Functional Band Gap of Wurtzite InN." Diola Bagayoko and Lashounda Franklin, Journal of Applied Physics, 97, 123708, 2005.

"Re-examination of the Ab-initio Calculation of the Electronic Structures of ZnSe, Ge, and GaAs." G. L. Zhao, L. Franklin, and D. Bagayoko. Submitted to Physical Review B, 2005.

Presentations (14)

December 13, 2006. Department of Physics, Cairo University, Cairo, Egypt. *"Predictive Calculations of Electronic and Related Properties of Materials:* The BZW Method. D. Bagayoko (presenter). Audience: Condensed matter researchers and graduate students.

June 2, 2006, Department of Physics, Beijing (Peking) University, Beijing, China. *"Ab-initio Predictions of electronic Properties of Materials: The Bagayoko, Zhao, and Williams (BZW)*

Method." D. Bagayoko (presenter) and G. L. Zhao. Audience: Researchers and graduate students, Department of Physics, University of Beijing.

June 9-11, 2005, Beijing, China. China International Conference on Nanoscience and Technology. *"Ab-initio Simulations of the Growth and Structural Properties of Short Carbon Nanobells."* G. L. Zhao, D. Bagayoko, and E. G. Wang.

June 9-11, 2005, Beijing, China. China International Conference on Nanoscience and Technology. *"A Universal Relation Between the Densities of States Near van Hove Singularities and the Effective Electron Masses in 1-Dimensional Semiconductors."* G. L. Zhao and D. Bagayoko.

March 15, 2006, APS March Meeting, Baltimore, Maryland, USA. *"Density Functional Band Gap of AlAs."* Hua Jin, Guanglin Zhao, and Diola Bagayoko.

March 15, 2006, APS March Meeting, Baltimore, Maryland, USA. *"Calculated, Optical Properties of Wurtzite InN."* D. Bagayoko, H. Jin, and G. L. Zhao.

March 15, 2006, APS March Meeting, Baltimore, Maryland, USA. *"Predictions of Electronic and Optical Properties of Cubic InN."* L. Franklin, H. Jin, G. L.Zhao, and D. Bagayoko.

March 15, 2006, APS March Meeting, Baltimore, Maryland, USA. *"Optical Properties of Aligned Carbon Nanotube Mats for Photonic Applications."* G. L. Zhao, D. Bagayoko, and L. Yang.

March 14, 2006, APS March Meeting, Baltimore, Maryland, USA. *"Ab-initio Simulations of the Growth of Short Carbon Nanobells."* G. L. Zhao, and D. Bagayoko.

March 25, 2005. Los Angeles, CA. March Meeting of the American Physical Society (APS). *"Structural, Elastic, and Electronic Properties of Deformed Carbon Nanotubes under Uniaxial Strain." A. Pullen SUBR & (Caltech),* G. L. Zhao, D. Bagayoko, and L. Yang (NASA), Bull. APS, Vol. 50, No. 1, Page 1420 (2005).

March 23, 2005. Los Angeles, CA. March Meeting of the American Physical Society (APS). *"Re-examination of Ab-initio Calculation of the Electronic Structure of Zn Se, Ge, and GaAs."* G. L. Zhao, L. Franklin, and D. Bagayoko, Bull. APS, Vol. 50, No. 1, Page 1073 (2005).

March 22, 2005. Los Angeles, CA. March Meeting of the American Physical Society (APS). *"True LDA Band Gaps of Wurtzite and Cubic Indium Nitride (w-InN and c-InN)."* D. Bagayoko, G. L. Zhao, and L. Franklin. Bull. APS, Vol. 50, No. 1, Page 617 (2005). Audience: Approximately 70 physical science researchers and graduate students.

February 18, 2005. Orlando, Florida, Disneyland. 2005 National Conference of the National Society of Black Physicists (NSBP) and of the National Society of Hispanic Physicists (NSHP). *"Local Density Functional Description of Electronic Properties of Wurtzite Zinc Oxide (ZnO)."* D. Bagayoko, G. L. Zhao, and L. Franklin. Audience: 17 faculty members, graduate students, and federal lab researchers.

February 17, 2005. Orlando, Florida, Disneyland. 2005 National Conference of the National Society of Black Physicists (NSBP) and of the National Society of Hispanic Physicists (NSHP). *"A Competitive Edge for Recruitment: The Versatility and Wonders of Physics."* D. Bagayoko. Audience: 20 faculty members, graduate students, and federal lab researchers.

Code Development

Another major component of our accomplishments in this reporting period stems from the development and refinement of the computer program package for wider utilization, including accurate total energy calculations. We have also developed a precise and concise user-manual that we are currently field-testing for effectiveness.

Research Training of Students

We have trained four (4) minority undergraduate students in the performance of the sophisticated calculations this project entails. These students are physics majors at SUBR. One of the students is the first author on the Physical Review article on electronic, elastic, and related properties of single walled carbon nanotubes.

CONCLUSIONS: We have implemented in a successful manner, as gauged by the publications and technical presentations, this project focused on "predictive calculations of properties of wide-gap and nano-semiconductors. Materials studied to date include GaN, ZnO, wurtzite InN, cubic InN, and several carbon nanotubes. Our results, in contrast to previous DFT or LDA calculations by other groups, are in excellent agreement with experiment. The significance of these results is underscored below and in the abstract.

SIGNIFICANCE: Our articles on electronic, structural, optical, and other properties of semiconductors and carbon nanotubes (Please see the attached list of publications) have profound implications, even for the study of nuclei. These papers resolved a problem dating back to the beginning of quantum. Indeed, we solved the woeful, theoretical underestimation of the band gaps of semiconductors and insulators as compared to measured values. **The resolution of this problem has some serious implications for the design and fabrication of semiconductor-based and nano-devices.** A collateral benefit stems from the fact that the method of solution also applies to the prediction of nuclear energy levels in the shell model, opening the way to theoretical explorations of possibilities of a population inversion and the actual construction of a *"gamma ray amplification by stimulated emission of radiation (graser)" device. We believe that no comments are needed on commercial and other applications of a graser.*

PATENT INFORMATION: Not Applicable

AWARD INFORMATION: Not Applicable

ATTACHMENTS: FULL TEXT OF PUBLICATIONS LISTED ABOVE

LIST OF PUBLICATIONS

Final Report, Grant No. N00014-05-1-0009
D. Bagayoko, Ph.D., and G. L. Zhao, Ph.D.
Department of Physics, Southern University and A&M College

Full copies of the following articles are provided below, in the order in which they are listed

"Density functional Calculations of the Growth and Structural Properties of Short Carbon Nanobells," G. L. Zhao and D. Bagayoko. Refereed Proceedings, International Conference, Swizerland, July 2006.

"Calculated Optical Properties of Wurtzite InN," H. Jin, G. L. Zhao, and D. Bagayoko. Accepted for publication, as submitted, in the Journal of Applied Physics (Accepted in December 2006)

"Predictions des Propriétés Electroniques des Atomes, Molécules, et Semi-conducteurs." D. Bagayoko. Proceedings, 2004 Malian Symposium of Applied Sciences (MSAS), Bamako, Mali. Pages 53-58. ISBN No. 951-42-8026-1.

"Optical Properties of Aligned Carbon Nanotube Mats for Photonic Applications." G. L. Zhao, D. Bagayoko and L.Yang. Journal of Appl. Phys. 99, 2006

"Density Functional Band Gaps of AlAs." H. Jin, G. L. Zhao, and D. Bagayoko. Phys. Rev. B73, 245214 (2006).

"Structural, Elastic, and Electronic Properties of Deformed Carbon Nanotubes under Uniaxial Strain." *A. Pullen,* G. L. Zhao, D. Bagayoko, and L. Yang. Physical Review B 71, 205410.

"Ab-initio Simulations of the Growth and Structural Properties of Short Carbon Nanobells." G. L. Zhao, D. Bagayoko, and E. G. Wang. Accepted for publication in the Proceedings of the 2005 China Conference on Nanoscience and Technology, Beijing, China, July 2005.

"A Universal Relation Between the Densities of States Near van Hove Singularities and the Effective Electron Masses in 1-Dimensional Semiconductors." G. L. Zhao and D. Bagayoko. Accepted for publication in the Proceedings of the 2005 China Conference on Nano-Science and Technology , Beijing, China, July 2005.

"LDA and LCAO-BZW Description of Electronic Properties of Wurtzite Zinc Oxide (w-ZnO)." Diola Bagayoko, Lashounda Franklin, and G. L. Zhao, accepted for publications in Proceedings of the 2005 National Conference of the National Society of Black Physicists (www.nsbp.org), Orlando, Florida.

"Predictions of Electronic, Structural, and Elastic Properties of Cubic InN." Diola Bagayoko, Lashounda Franklin, and G. L. Zhao, Journal of Applied Physics 96, 4297-4301, 2004.

"Density Functional Band Gap of Wurtzite InN." Diola Bagayoko and Lashounda Franklin, Journal of Applied Physics, 97, 123708, 2005.

"Re-examination of the Ab-initio Calculation of the Electronic Structures of ZnSe, Ge, and GaAs." G. L. Zhao, L. Franklin, and D. Bagayoko. Submitted to Physical Review B, 2005.

Ab-Initio Density Functional Calculations of the Growth and Structural Properties of Short Carbon Nanobells

G L Zhao and D Bagayoko

Department of Physics, Southern University and A & M College
Baton Rouge, Louisiana 70813, USA

Corresponding author's e-mail address: zhao@grant.phys.subr.edu

Abstract. We performed ab-initio density functional calculations to study the structural and growth properties of short carbon nanobells. We used a real space approach and the linear combination of atomic orbitals (LCAO) formalism. In the nitrogen-doped carbon nanobells, the nitrogen atoms that are attracted to the open-edge sites of the carbon nanobells play an important role in the growth of the short carbon nanostructures. We present the calculated electronic structure of the short nanobells. The calculated local density of states of the nanobells revealed field emission characteristics that agree with experimental observations.

1. Introduction

Carbon nanostructures present interesting properties with a great potential of applications. Particularly, short carbon nanotubes or carbon nanobells present excellent field-emission properties that have attracted a great interest for applications.[1-8] Experiments demonstrated that the nitrogen-assisted synthesis can grow carbon nanofibers on a large scale.[9-12] Such carbon nanofibers exhibit a "bamboo-like" structure. Distinctively, a great part of the bamboo-like nanofibers consists of short carbon nanobells. Individual nanobells are self-contained and stack one on top of the other to create a long nanofiber. The carbon nanobells may be viewed as short nanotubes such that their lengths are of the same order as their diameters. The electronic structure of the short carbon nanobells is substantially different from that of the pure and long carbon nanotubes because of the quantum effects inherent to their sizes. The nanobells exhibit novel electron field emission properties with a turn-on field of electron emission as low as $0.8 V / \mu m$.[9,13] We performed ab-initio density functional calculations, aiming to understand the growth, structural, and electronic properties of short carbon nanobells.

2. Method

Although the experimental synthesis of carbon nanobells produced samples of various sizes, measurements revealed that the atomic structure of the bamboo-like morphology in thick nanobells is similar to that of the thinner ones.[9] Experiments also revealed that adjacent nanobells do not have a firm contact, but instead the closed end of one nanobell is weakly inserted into the open end of another. Single nanobells can be easily separated from other

parts of the nanofiber.[10] Hence, our ab-initio calculations will focus on single nanobells. The weak interaction between adjacent carbon nanobells may be included as a perturbation in further studies in modeling the bamboo-like morphology of the nanofibers. We constructed a prototypical carbon nanobell as a model to simulate the general structure of short carbon nanobells. Figure 1 presents the calculated images of the electron density distribution of a prototypical carbon nanobell in real space. The prototypical carbon nanobell includes 150 atoms and consists of half of the C240 fullerene with 30 extra atoms on the bell. Its length and diameter are 8.5 and 7.4 $\mathring{A}$, respectively. Although the size of this prototypical carbon nanobell may differ from that of fabricated samples, their fundamental features are similar. These features include the structural properties of the open-edge, the wall, and the closed cap of the nanobells.

Figure 1. The calculated images of the electron density distribution in real space for a prototypical carbon nanobell that is viewed from different directions

Our ab-initio calculations are based on the density functional theory of Hohenberg-Kohn and Kohn-Sham.[14,15,16,17,18] In the linear combination of atomic orbitals (LCAO) method, we solved the Kohn-Sham equations self-consistently by employing the Rayleigh-Ritz variational process. [19,20] In the self-consistent calculations for the electronic structure of short CN_x nanobells, we employed an extended basis set that includes atomic orbitals of C(1s2s3s 2p3p) and N(1s2s3s 2p3p). Here C(3s 3p) and N(3s 3p) are extra orbitals that are used to augment the basis set to account for possible charge diffusion and polarization in the short nanobells. The real space approach of the LCAO method enables us to complete the required computations using our SiliconGraphics Origin2000 that is equipped with 4 GB RAM (memory).

3. Results

3.1. Relaxed Atomic Structure near the Open-Edge of the Short Carbon Nanobell

The open-edges of carbon nanobells play an important role in their electronic properties. The structure near the open edge of the carbon nanobell is different from that in the inner wall and the closed cap. We performed total energy minimization to identify the atomic structure near the open-edge of the prototypical carbon nanobell. The calculated C-C bond length on the

first atomic ring at the open-edge of the carbon nanobell is $1.37\,\mathring{A}$, which is much shorter than the C-C bond length of $1.415\,\mathring{A}$ in the inner atomic rings of the bell. This reduction of the C-C bond length for the carbon atoms at the open-edge sites is a result of the reduction in coordination number. The calculated bond length of the carbon atoms on the first atomic ring to the carbon atoms on the second ring is $1.40\,\mathring{A}$, which is not much different from that in the inner rings, away from the open-edge of the nanobell. This result indicates that the effect of further relaxation of the third atomic ring and inner rings would be insignificant.

3.2. A Possible Growth Mechanism of Carbon Nanobells

The growth mechanism of the carbon nanobells remains a difficult problem. There are probably two major growth models. [1] The first one assumes that the carbon atoms are added at the open-ends of the nanobells.[1,11] The second one involves the C_2 absorption process that is assisted by the pentagonal defects on the closed caps. [1] Although both models are very interesting, we have technical difficulties using density functional computations to simulate the second growth model. We successfully performed local density functional computations to test the first growth mechanism. Because of the active dangling bonds of carbon atoms at the open-edge of nanobells, there is a high possibility that carbon atoms can be attracted to these sites for growth to occur. We calculated the total energies in the following two cases. In the first case, a ring of 20 carbon atoms attaches to the open-edge of the carbon nanobell at a bond-length of $1.415\,\mathring{A}$. In the second case, these 20 carbon atoms are free. The calculated total energy in case I is substantially lower than the corresponding value in case II. The total energy difference, which may also be defined as the cohesive energy of the carbon atoms in the first growth model, is 4.7 eV/atom. In this growth model, see Figure 1, C_2 dimers are absorbed at the active dangling bond sites at the open end of the carbon nanobell. A C_2 dimer that deposits on the open-edge of the bell forms one covalent bond on the same atomic ring. Each of the C atoms also forms one covalent bond with the C atom of the next atomic ring and remains an active dangling bond towards the open-space. This growth model is consistent with previous analysis of experimental results.[11,13,21] Although we cannot rule out the second growth model (growth on the closed cap of carbon nanobells), our calculations presented clear evidence that the first growth mechanism is highly possible.

3.3. Nitrogen-Doped Carbon Nanobell

Experimental results indicated that the growth of the short carbon nanobells is highly dependent on the nitrogen concentration in the gas mixture during the synthesis.[9,10] Without nitrogen atoms in the growth gas mixture under the same conditions, long and pure carbon nanotubes, without the "bamboo-like" morphology, are produced. However, it was not clear why the nitrogen atoms could turn the growth of the would-be long carbon nanotubes into that of short carbon nanobells. We performed total energy calculations to study the nitrogen-doped carbon nanobells (CN_x nanobells). Since nitrogen atoms can also form the planar sp^2-hybrid,[22] we studied the substitutional doping of nitrogen atoms in the CN_x nanobells. The substitutional doping of nitrogen atoms in CN_x nanobells was also proposed from the analysis of experimental results.[13]

We first replaced carbon atoms with nitrogen atoms at the open-edge of the prototypical nanobell. We compared the total energies in the two cases. In the first case, computations are carried out for the pristine carbon nanobell in the presence of ten free atoms

of nitrogen. In the second case, ten nitrogen atoms replace ten carbon atoms on the open-edge and the substitutionally N-doped nanobell is in the presence of ten free atoms of carbon. The calculated total energy in the second case is lower than that in the first case by an amount of 0.5 eV per atom, without relaxing the structure. We then performed total energy calculations and identified the atomic positions of the relaxed structure of the nitrogen-doped nanobell from the total energy minimization. The calculated C-N bond length in the first atomic ring at the open-edge of the nanobell is 1.376 $\mathring{A}$. The bond-length, from the nitrogen atoms of the first atomic ring to the carbon atoms of the second atomic ring, is 1.377 $\mathring{A}$. They are close to the length of the partially double C-N bond (1.352 $\mathring{A}$) in heterocyclic systems.[23] The C-C bond length from the first atomic ring to the second ring is 1.397 $\mathring{A}$. The total energy of the nitrogen-doped nanobell, in the relaxed structure, is lower than that of the undoped one by 0.72 eV per atom.

We also studied the substitutional doping with nitrogen atoms (for carbon atoms) in the wall (away from the open-edge and the closed cap) of the prototypical carbon nanobell. We used the same computational procedure as discussed above. The calculated total energy of the N-doped nanobell, at the wall position, is much higher than that of the undoped bell by an amount of 5 eV per atom. This result indicates that the substitutional doping with nitrogen in the wall of carbon nanobells is not energetically favored.

These calculated results for the nitrogen-doped nanobells in the prototypical model thus indicate that the dopant nitrogen atoms prefer to stay at the open edge of the nanobell as opposed to being in the wall (i.e. lower rings) of the nanobell. Once there are enough nitrogen atoms on the open edge of the nanobell, carbon atoms cannot attach to the open-edge of the CN_x nanobell. Such an attachment will result in nitrogen atoms being in inner rings other than that at the open-edge, resulting in a configuration that is not favored energetically. Consequently, nitrogen atoms act as the stopper of the growth of the carbon nanobell. This growth mechanism for the nitrogen-doped carbon nanobells and the effect of the nitrogen atoms in the growth process agree with the observations from experiments.[9,10,11,13]

We present the calculated local density of states (LDOS) of the CN_x nanobell in Figure 2. The dopant nitrogen atoms stay at the open-edge sites in the prototypical nanobell. The LDOS from the nitrogen and carbon atoms on the first atomic ring at the open-edge of the nanobell are shown in the first and the second panels of Figure 2, respectively. There is no N atom on other atomic rings away from the open-edge of the nanobell. Figure 2 clearly shows that the N and C atoms on the first atomic ring at the open-edge of the nanobell have the dominant contribution to the electronic states around the Fermi level. The LDOS at the Fermi level, from the N and C atoms on the first atomic ring at the open-edge, are 0.56 and 0.71 states per eV per atom, respectively. The contribution, from the second atomic ring near the open-edge, to the LDOS at the Fermi level is 0.23 states per eV per atom. The third atomic ring and the inner rings, that include the closed cap, have a much smaller contribution to LDOS at the Fermi level, at about 0.08 states per eV per atom. Thus, electrons will be emitted from the atomic sites near the open-edge of the nanobell in field-emission experiments. The real nanobell samples in experimental studies mostly involve multilayers of graphite sheets and the nanobells stacked one on top of the other. The weak interactions between graphite layers in these nanobells and that between the bells may further broaden the electronic energy levels.

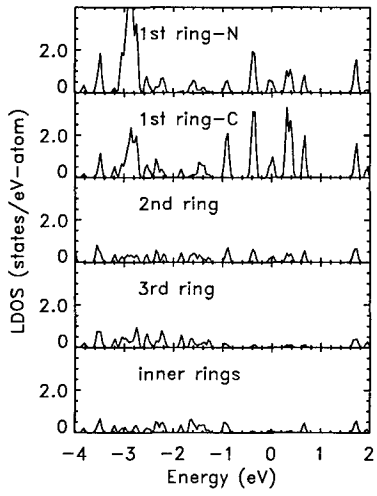

Figure 2. The calculated local density of states of electrons of a nitrogen-doped carbon nanobell. The 1st ring-N and –C refer to the nitrogen and carbon atoms on the first atomic ring at the open-edge of the nanobell. The 2nd and 3rd rings refer to the second and third atomic rings near the open-edge. The inner rings refer to the atomic sites away from the open-edge, including the closed cap. The Fermi level is at 0.0 eV.

4. Conclusion

In conclusion, we performed ab-initio density functional calculations to simulate the growth, structural, and electronic properties of prototypical carbon nanobells. In the nitrogen-doped carbon nanobells, nitrogen atoms that are attracted to the open-edge of the nanobells may play a role of stopper of the growth of the nanostructures. The calculated local densities of states of the CN_x nanobells indicate that electrons are most likely emitted from the atomic sites near the open-edge of the carbon nanobell in field-emission experiments. This result agrees with experimental observations.

Acknowledgements: This work was funded in part by the US Department of the Navy, Office of Naval Research (ONR Award No: N00014-05-1-0009), by US National Science Foundation (Award No. CCF-0508245), and by US NASA (Award No. NCC 2-1344).

References

[1] Dresselhaus M S, Dresselhaus G, and Eklund P C 1996 Science of Fullerenes and Carbon Nanotubes, (Academic Press, New York).
[2] de Heer W A, Châtelain A, Ugarte D 1995 Science, **270,** 1179.
[3] Rinzler A G, et al 1995 Science, 269, 1550.
[4] Wang Q H, et al 1997 Appl. Phys. Lett. **70**, 3308
[5] Wang Q H, et al 1998 Appl. Phys. Lett. **72,** 2912.
[6] Chen Y, et al 1998 Appl. Phys. Lett. **73, 2119**.
[7] Dean K A and Chalamala B R 2000 Appl. Phys. Lett. **76, 375**.
[8] Bonard J M, et al 1998 Phys. Rev. Lett. **81**, 1441.
[9] Ma X, et al 1999 Appl. Phys. Lett. **75**, 3105.

[10] Ma X, et al 2000 Appl. Phys. Lett. **77, 4136**.
[11] Ma X and Wang E G 2001 Appl. Phys. Lett. **78**, 978.
[12] Wang E G , et al 2003 Carbon **41**, 1827.
[13] Zhong D Y, Liu S, Zhang G Y, Wang E G 2001 J. of Appl. Phys. **89**, 5939.
[14] Hohenberg P and Kohn W 1964 *Phys. Rev.* **136**, B864; Kohn W and Sham L J 1965 *Phys. Rev.* **140**, A1133.
[15] Zhao G L, Bagayoko D, and Yang L 2004 Phys. Rev. B **69**, 245416.
[16] Callaway J and March N H 1984 *Solid State Physics*, vol. 38, Edited by H. Ehrenreich, D. Turnbull, and D. Seitz, (Academic Press, New York), p.135.
[17] Zhao G L, Bagayoko D, and Wang E G 2003 Modern Physics Letters B, **17**, 375.
[18] Bagayoko D, Zhao G L, Fan J D, and Wang J T 1998 *Journal of Physics: Condensed Matter*, **10** , 5645.
[19] Mikhlin S. G 1971 *The Numerical Performance of Variational Methods*, (Wolters-Noordhoff Publishing), ch.1, 2, & 7.
[20] Gould S H 1957 Variational *Methods for Eigenvalue Problems*, (University of Toronto Press), Ch. 2.
[21] Gavillet J, Loiseau A, Journet C, Willaime F, Daucastelle F, and Charlier J C 2001 Phys. Rev. Lett. **87**, 275504.
[22] Harrison W A 1980 Electronic Structure and the Properties of Solids, (W. H. Freeman and Company, San Francisco), p. 91.
[23] CRC Handbook of Chemistry and Physics, 1990 Edited by R. C. Weast. D. R. Lied, M. J. Astle, and W. H. Beyer, (CRC Press, Boca Raton, Florida), p. F-188.

Calculated, Optical Properties of Wurtzite InN

H. Jin, G. L. Zhao, and D. Bagayoko*

Department of Physics, Southern University and A & M College

Baton Rouge, Louisiana 70813

Abstract

We report ab-initio, self-consistent results for the dielectric function of wurtzite indium Nitride (w-InN). Our calculations employed a local density approximation (LDA) potential, the linear combination of atomic orbitals (LCAO), and the Bagayoko, Zhao, and Williams (BZW) method. Our findings agree very well with recent measurements up to photon energies of 6 eV. This excellent agreement shows the correct description, by the LDA-BZW method, of the relative separations between upper valence bands and low-lying conduction bands, in general, and corroborates our previous result of 0.88 eV for the intrinsic, fundamental band gap of w-InN, in particular. We also report results of simulations of the effect of high electron doping on the optical properties of InN.

* Corresponding author. Tel.: 225 771-2730; fax: 225 771-4341.
Email address: bagayoko@phys.subr.edu

features below 1 eV and exhibit a clear indication of an absorption edge around 2 eV,[2-4] in accordance with the findings of the experimental Group I for the band gap. In contrast, the second set[5-10] of experiments not only shows the onset of absorption below 1 eV but also shows no features around 2 eV. A motivation for this work is to resolve the above discrepancy between two sets of experimental measurements of the dielectric functions (i.e., imaginary and real parts) of the w-InN. The above excellent results of the DFT-BZW approach, for the band gap and the effective mass, portend its capability in resolving this second controversy surrounding the optical properties of w-InN by comparing the calculated dielectric function, obtained with the *ab-initio*, self-consistent, DFT-BZW bands, to experimental measurements. While the results of these calculations of the optical properties of w-InN are expected to show an absorption edge type feature around 0.8 eV, it is not a priori known whether or not they will also exhibit another feature around 2 eV, as suggested by the first set of measurements.

While the above discrepancy amply points to the need for this work, this need is further exacerbated by the fact that previous calculations entailed either fittings[11] to models of the dielectric function or a scissors-type approximation to adjust the calculated imaginary part of the dielectric function[12] or the calculated band gaps.[13-16] The modeling work of Djurišić and Li[11] and the calculations of Abbar et al.[13] generally agreed with the first set of measurements, i.e., with an absorption onset around 2 eV, as per the imaginary part of the dielectric function. Furthmüller et al.[15] and Bechstedt et al.[16], following scissors-type adjustments to 0.81 eV of their otherwise negative, calculated band gap, reproduced dielectric functions in general agreement with the results of the second set of measurements.

III. Results: Calculated Dielectric Functions

The calculated $\varepsilon_2(\omega)$ for wurtzite InN was resolved into two components, i.e., $\varepsilon_{2xy}(\omega)$ and $\varepsilon_{2z}(\omega)$ that are the averages of the spectra for polarizations perpendicular and parallel to the c-axis, respectively. Figures 1a and 1b show $\varepsilon_{2xy}(\omega)$ and $\varepsilon_{2z}(\omega)$, respectively, along with recent experimental data of Goldhahn et al.[6] The peak positions, shapes, and intensities of our calculated $\varepsilon_2(\omega)$, in both polarization directions, are found to be in agreement with experiment up to photon energies of 6 eV, especially for the component in the xy plane. The calculated dielectric functions exhibit the anisotropy revealed by experimental measurements. The first peaks at 0.88 eV , for $\varepsilon_{2xy}(\omega)$, and at 0.85 eV, for $\varepsilon_{2z}(\omega)$, indicate the onset of band edge absorption. They are measures of the direct optical band gap. Our minimum, calculated band gap is 0.75 eV, which is lower than the actual theoretical minimum of 0.88 eV[1] due to constraint stemming from using the same number of orbitals of the respective s, p, and d states of In and N. Due to this restriction that is currently inherent to our optical property calculation program, the basis set for N, in the self-consistent calculations performed here, is slightly larger than the optimal one.[1] This value of 0.75 eV still falls within the range of 0.7 to 1.0 eV, as per the experimental Group II noted above. While the above agreement of our calculated results with experiment is expected in the vicinity of the calculated band gap, the absence of features indicative of absorption, around 2 eV, is an important result. It partly settles the debate between experiments in Set I and Set II by establishing that high quality w-InN, in the absence of high free carriers concentrations, behave as per the findings of experiments in Set II. Calculated and experimental peak positions of the imaginary part of the dielectric function, along with the possible optical interband transitions, are listed in Table I. Besides the gap structure, $\varepsilon_{2xy}(\omega)$ shows six peaks which are related to critical points of the band structure (CPBS), while $\varepsilon_{2z}(\omega)$ exhibits three CPBS. The possible optical transitions

shifted $\varepsilon_2(\omega)$ spectra. A typical calculation result is shown in Figure 3. We depict the calculated $\varepsilon_2(\omega)$ in the two polarization directions, along with the results of an experiment[2] in Set I, in panels 3a and 3b, respectively[6]. The optical absorption edge of 1.9 eV, the previous band gap, was obtained when we increased the Fermi level from the top of valence band (TOV) to 1.85 eV above the TOV. The solid lines, in Figures 3a and 3b, represent the results of the simulation. Experiment and simulation appear to agree reasonably for photon energies up to 5 eV.

V. Summary

In summary, our ab-initio, self-consistent, DFT-BZW calculations have practically reproduced the experimental values of the dielectric function of wurtzite InN for photon energies up to 6 eV. DFT-BZW calculations are fundamentally for the description of the ground state. Hence, the disagreement between DFT-BZW results and experiments, for high photon energies, was expected. Given that the work functions of many semiconductors is around or below 6 eV, the above disagreement for high photon energies may not be a serious handicap for InN. For other semiconductors, a key issue consists of the determination of the photon energy up to which DFT-BZW and experiment agree. For photon energy above 6 eV, the CPBS still agree fairly with experiment, as per the values in Table I. The optical absorption edge of 1.9 eV was simulated by increasing the Fermi Level into the conduction band. The agreement between the results of this simulation and optical properties measurements of w-InN samples with a large band gap (i.e., around 2 eV) appears to confirm that the increased Fermi level, as a result of high electron doping, is responsible for the large band gaps.

References

[1] D. Bagayoko, and L. Franklin, J. Appl. Phys. **97**, 123708 (2005).

[2]Q. Guo, O. Kato, M. Fujisawa, and A. Yoshida, Solide State Commun. **83**, 721 (1992).

[3]Q. Guo, H. Ogawa, and A. Yoshida, J. Electron Microscopy and Related Phenomena **79**, 9 (1996).

[4]H. F. Yang, W. Z. Shen, Z. G. Qian, Q. J. Pang, H. Ogawa, and Q. X. Guo, J. Appl. Phys. **91**, 9803 (2002).

[5]Q. Kasic, E. Valcheva, B. Monemar, H. Lu, and W. J. Schaff, Phys. Rev. B **70**, 115217 (2004).

[6]R. Goldhahn, A. T. Winzer, V. Cimalla, O. Ambacher, C. Cobet, W. Richter, N. Esser, J. Furthmüller, F. Bechstedt, H. Lu, and W. J. Schaff, Superlattices and Microstructures **36**, 591 (2004).

[7]R. Goldhahn, P. Schley, A. T. Winzer, M. Rakel, C. Cobet, N. Esser, H. Lu, and W. J. Schaff, J. Crystal Growth **288**, 273 (2006).

[8]H. Ahn, C. –H. Shen, C. –L. Wu, and S. Gwo, Thin Solid Films **494**, 69 (2006).

[9]J. Wu, W. Walukiewicz, S. X. Li, R. Armitage, J. C. Ho, E. R. Weber, E. E. Haller, Hai Lu, William J. Schaff, A. Barcz, and R. Jakiela, Appl. Phys. Lett. **84**, 2805 (2004).

[10]W. Walukiewicz, S. X. Li, J. Wu, K. M. Yu, J. W. Ager III, E. E. Haller, Hai Lu, and William J. Schaff, J. Crystal Growth **269**, 119 (2004).

[11]Aleksandra B. Djurišić and E. Herbert Li, J. Appl. Phys. **85**, 2848 (1999).

[12]C. Persson, R. Ahuja, A. Ferreira da Silva, and B. Johansson, J. Phys.: Conden. Matt. **13**, 8945 (2001).

[13]B. Abbar, B. Bouhafs, H. Aourag, G. Nouet, and P. Ruterana, Phys. Stat. Solidi B **228**, 457 (2001).

[14]N. E. Christensen, I. Gorczyca, Phys. Rev. B **50**, 4397 (1994).

Table I. Peak positions (in eV) of the imaginary part of the dielectric function $\varepsilon_2(\omega)$ for InN.

Exp.[a] ε_{2xy}	Exp.[a] ε_{2z}	Cal.[b] ε_{2xy}	Cal.[b] ε_{2z}	Optical Transition	Energy (eV)
4.88*		4.72		$\Gamma_{4,5v}$ - Γ_{2c}	4.62
5.35	5.38	5.54	5.54	M_{1v}-M_{1c}	5.64
6.05*		6.16	6.62	$L_{1,2v}$-$L_{1,2c}$	6.09
				$L_{3,4v}$-$L_{1,2c}$	6.18
				M_{2v}-M_{1c}	6.52
				$A_{5,6v}$-$A_{1,2c}$	6.57
7.87	7.63	8.33*		M_{2v}–M_{2c}	7.94
				M_{3v}–M_{2c}	8.49
8.60		8.85	8.95	$\Gamma_{4,5v}$ – Γ_{3c}	8.60
				A_{1-4v}-$A_{3,4c}$	8.72
				K_{1v}-K_{1c}	8.87
				K_{1v}-$K_{2,3c}$	8.91
	9.44	9.51*	9.90	$L_{3,4v}$-$L_{3,4c}$	9.34
				M_{4v}–M_{2c}	9.52

*Shoulders.

[a]Experiment: Spectroscopic ellipsometry on MBE grown InN film.[6]

[b]Our calculation results.

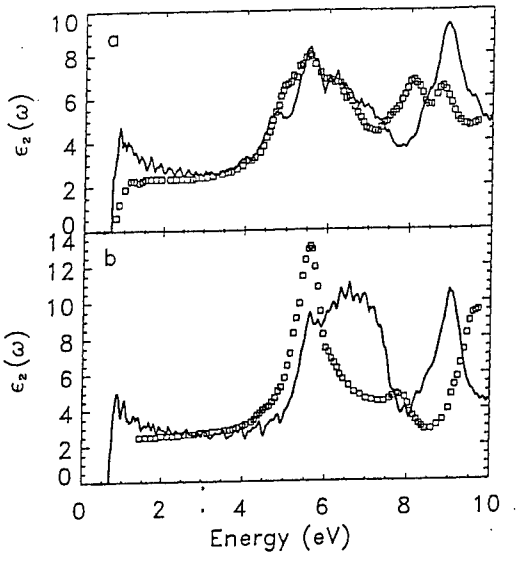
a
b
$\epsilon_2(\omega)$
$\epsilon_2(\omega)$
Energy (eV)

PREDICTIONS DES PROPRIETES ELECTRONIQUES DES ATOMES, MOLECULES, ET SEMI-CONDUCTEURS

Diola Bagayoko, Ph.D.
(Bagayoko@aol.com)
Professeur Distingué de Physique et
Directeur de l'Académie de Tombouctou
Département de Physique
Southern University and A&M College
Baton Rouge (SUBR), Louisiane, USA

Abstract

Nous rapportons des résultats inédits, sur les bandes d'énergies de certains matériaux, obtenus avec la méthode de Bagayoko, Zhao, et Williams (BZW). Les actes du premier Symposium Malien des Sciences Appliquées, en 2000, contiennent une description détaillée de la méthode BZW, en français. Des références citées ci-dessous décrivent la méthode en anglais. La méthode a résolu un problème qui date du début du 20ième siècle. Une motivation pour cet article consiste à encourager des collègues africains à utiliser la méthode pour se placer à la frontière de la description quantique des propriétés électroniques des atomes, molécules, et solides, avec une capacité de prédire les dites propriétés, à commencer par les fossés d'énergie ou de bandes.

We report new results, on energies bands of some materials, obtained with the Bagayoko, Zhao, and Williams (BZW) method. The Proceedings of the first Malian Symposium of Applied Sciences (MSAS), in 2000, contain a detailed description of the BZW method in French. References cited below (1-11) describe the method in English. The method has resolved a problem dating from the beginning of the 20th Century. One motivation for this article consists of encouraging some African colleagues to utilize the method in order to place themselves at the forefront of the quantum mechanical description of electronic properties of atoms, molecules, and solids, with a capacity of predicting these properties, beginning with energy gaps and band gaps.

Introduction

Les Actes du Symposium Malien des Sciences Appliquées de 2000 donnent une description détaillée de la méthode de Bagayoko, Zhao, et Williams. Le problème résolu par la méthode consistait, durant la plupart du 20ième siècle, d'un désaccord flagrant entre les résultats expérimentaux et les valeurs calculées de la hauteur ou de l'épaisseur des bandes interdites des semi-conducteurs. Cette hauteur, pour un système donné, consiste en la différence entre le niveau vide le plus bas et le niveau occupé le plus élevé ; nous l'appelons le fossé d'énergie (pour les atomes, molécules, et autres systèmes finis) ou fossé de bande pour les semi-conducteurs et les isolants. Ce problème, pendant un siècle, a empêché la théorie (i.e., les calculs quantiques) de bien informer et de guider la conception et la fabrication d'instruments et d'appareils électroniques de tout genre. En effet, pour toute application d'un atome, d'une molécule, ou d'un semi-conducteur, le fossé d'énergie ou de bande est très souvent incontournable. Par exemple, l'absorption d'une radiation électromagnétique par un semi-conducteur demande que l'énergie de la radiation soit égale ou plus grande que le fossé de

Des Nouveaux Résultats de la Méthode BZW

Les nouveaux résultats de la méthode BZW comprennent les solutions des problèmes illustrés dans les tables ci-dessus. En effet, dans les sources indiquées pour les données dans ces tables, Bagayoko et collaborateurs ont rapporté des fossés d'énergies pour l'oxide de zinc (ZnO) et pour InN qui sont en accord avec l'expérience. Dans le cas de InN, notre résultat de 0.88 eV est en accord avec le group 2 d'expérience. Nous avons trouvé une valeur de 3.28 eV pour ZnO, bien en accord avec l'expérience et plus du double de la plupart des autres valeurs théoriques obtenues sans la méthode BZW. La table suivante montre d'autres résultats de la méthode BZW pour InN, dans les réseaux wurtzite et cubique.

Band Gaps (Fossés de Bande)		
	Calculated	**Experiment**
Wurtzite (w-InN), LDA-BZW a = 3,544 Å, c = 5,718 Å, u = 0,3790	0,88 eV	0,7-1,0 eV As per Exp. Group 2
Wurtzite (w-InN), GGA-BZW a = 3,544 Å, c = 5,718 Å, u = 0,3790	0,81 eV	
Zinc Blende (c-InN), LDA-BZW a =5,017 Å (Equilibrium)	0,65 eV	Not Available
Zinc Blende (c-InN), LDA-BZW a =4,98 Å (Experimental)	0,74 eV	Not Available

Effective Mass (Masse Effective)			
	Directions		**Experiment**
Wurtzite (w-InN), LDA-BZW a = 3,544 Å, c= 5,718 Å, u = 0,3790	**Γ - M**	0,088 mo	0,07 estimated with a band gap of 0,7 eV
	Γ - A	0,082 mo	
	Γ- K	0,088 mo	
Wurtzite (w-InN), GGA-BZW a = 3,544 Å, c = 5,718 Å, u = 0,3790	**Γ - M**	0,081 mo	0,07 estimated with a band gap of 0,7 eV
	Γ - A	0,077 mo	
	Γ- K	0,082 mo	
Zinc Blende (c-InN), LDA-BZW a = 5,017 Å (Equilibrium)	**Γ - L**	0,065 mo	Not Available
	Γ - X	0,066 mo	
	Γ- K	0,066 mo	
Zinc Blende (c-InN), LDA-BZW a = 4,98 Å (Experimental)	**Γ - L**	0,076 mo	Not Available
	Γ - X	0,073 mo	
	Γ- K	0,073 mo	

s'avèrent nécessaires dans de nombreux projets de recherche. Inutile d'ajouter que les résultats de ces calculs peuvent être publiés dans les journaux les plus réputés.

Nous estimons que la formation pour l'exécution de ces calculs ne prend que quelques mois. Un seul chercheur formé en la matière peut encadrer plusieurs étudiantes (ou étudiants) de doctorat en même temps! Ajoutons que les diverses applications soulignées ci-dessous ont trait non seulement aux secteurs économiques, industriel, et autres (i.e., pharmaceutiques), mais aussi à ceux de la défense et de la sécurité ou sûreté nationales.

Finalement, nous répétons la conclusion dans les Actes de MSAS 2000 : Apres avoir résolu le problème précité (la catastrophe des fossés d'énergie ou de bande), la méthode BZW a ouvert la voie pour

- **La prédiction de nouvelles molécules** (larges ou petites, inorganiques ou organiques) ;
- **La prédiction des fossés d'énergie ou de bande (band gaps) des matériaux** (pour guider la conception et la fabrication d'instruments électroniques divers--des plus simples aux plus complexes) ;
- **Une compréhension approfondie de la structure des noyaux atomiques ;**
- **L'amélioration des simulations** en fournissant des paramètres pour les formes d'énergie potentielle utilisées par les simulations de la dynamique moléculaire (DM or MD) ou de la méthode de Monte Carlo (MC) ; et
- **Un avancement fondamental de notre connaissance de la matière (nucléaire, atomique, moléculaire, et condensée)** et des limitations réelles de la théorie de la fonctionnelle de la densité ainsi que de celles d'autres théories qui sont supposées la corriger ou la remplacer. Avant notre travail en 1998, la théorie de la fonctionnelle de la densité était blâmée par tous pour le flagrant désaccord entre les valeurs calculées et les valeurs mesurées des fossés d'énergie ou de bande.

Prière de bien réfléchir sur les implications immédiates et futures de la méthode BZW pour les industries (des semi-conducteurs, du noyau atomique, de la biotechnologie, et surtout de la nano-technologie naissante). A l'échelle du nanomètre, les effets quantiques sont non seulement omniprésents, mais aussi ils ne sont pas négligeables !

Remerciements

Notre recherche a été financée par le Département Naval des Etats Unis D'Amérique et son Bureau de la Recherche Navale (ONR, Award No. N00014-04-1-0587), la Fondation Nationale de la Science des USA (NSF, Award No. HRD 0000272), et par la NASA (Award No. NCC 2-1344 et No. NNG 05G146G). *Mes collaborateurs sont Dr. G. L. Zhao, Mr. Troy D. Williams, et Ms. Lashounda Franklin (ces deux derniers étaient mes étudiants).*

Optical properties of aligned carbon nanotube mats for photonic applications

G. L. Zhao[a] and D. Bagayoko
Department of Physics, Southern University and A & M College, Baton Rouge, Louisiana 70813

L. Yang
Eloret, NASA Ames Research Center, MS230-3, Moffett Field, California 94035

(Received 21 September 2005; accepted 31 March 2006; published online 8 June 2006)

We studied the optical properties of the aligned carbon nanotube (16, 0), (10, 0), and (8, 4) mats for photonic device applications. We employed *ab initio* density functional potentials and utlized the linear combination of atomic orbital formalism. We calculated the electronic structure of the carbon nanotube mats and the real and imaginary parts of the dielectric functions as functions of the photon energy. The calculated dielectric functions of the aligned carbon nanotube mats show a strong anisotropy when the electric field of the light is parallel or perpendicular to the tube axes. Especially, there are strong peaks in the imaginary part of the dielectric function near the absorption edges, when the electric field of the light is parallel to the carbon nanotube axes. The unusual optical properties of the semiconducting carbon nanotube mats present an opportunity for applications in electro-optical devices in the infrared energy region. © *2006 American Institute of Physics.*
[DOI: 10.1063/1.2201738]

I. INTRODUCTION

Carbon nanotubes possess unique electronic properties that are very useful for building electro-optical devices at nanometer scales. Recently, Wu *et al.* reported ultrathin, transparent, optically homogeneous, electrically conducting films of pure single-walled carbon nanotubes.[1] The films exhibit optical transmittance comparable to that of commercial indium tin oxide in the visible spectrum, but far superior transmittance in the technologically relevant 2–5 μm infrared spectral band. These characteristics indicate broad applicability of the films for electrical coupling in photonic devices. Kim *et al.* reported highly polarized absorption and photoluminescence of stretch-aligned single-walled carbon nanotubes dispersed in gelatin films.[2] The highly polarized absorption and photoluminescence are attributed to interband optical transitions in the single-walled carbon nanotubes (SWCNTs). The realization of highly aligned and luminescent SWCNT thin films should contribute to the development of SWCNTs as optoelectronic materials. Li *et al.* also reported polarized optical absorption spectra of single-walled 4 Å carbon nanotubes arrayed in the channels of an AlPO4-5 single crystal.[3] The measured absorption spectra agreed well with the *ab initio* calculations based on the local density functional approximation. Carbon nanotubes may also be used in optical limiting, nonlinear optical devices, and other applications[4–10]

Guo *et al.* reported the linear and nonlinear optical properties of individual carbon nanotubes, utilizing full-potential projected augmented wave (PAW) method.[11] The calculations were based on *ab initio* density functional calculation within the local density functional approximation (LDA). A supercell geometry was adopted so that the nanotubes are aligned in a square array with the closest distance between adjacent nanotubes being at least 6 Å. They performed test calculations with larger intertube distances and no discernable differences were found. In their work, they aimed to study the optical properties of isolated or nearly isolated carbon nanotubes.

Machon *et al.* performed *ab initio* density functional calculations for the optical properties of 4 Å diameter single-walled carbon nanotubes.[12] The calculated optical properties confirmed the experimental results of Li *et al.*[3] for the strong anisotropy of the optical response of carbon nanotubes.

In optoelectronic applications, a large number of carbon nanotubes will be assembled in a desired form. As identified in the experimental studies, single-walled carbon nanotubes are self-assembled in a triangular lattice in bundles, strands, or mats.[13,14] The photonic devices based on carbon nanotubes can take advantage of the strong anisotropy of optical properties of SWCNTs under polarized light. This can be achieved by aligning the SWCNTs in a certain direction to form carbon nanotube mats. In this work, we aimed to study the optical properties of aligned carbon nanotube mats (CNTMs), using *ab initio* density functional calculations. We utilized the computational method of the linear combination of atomic orbital (LCAO) formalism. We calculated the optical properties of various CNTMs that were constructed from semiconducting SWCNTs. As a further pursuit of the applications of nanodevices, we demonstrate in this work that the aligned carbon nanotube mats will have relevant properties for photonic applications.

II. METHOD

We performed *ab initio* quantum calculations that are based on the density functional theory of Hohenberg-Kohn

[a]Author to whom correspondence should be addressed. Electronic mail: zhao@grant.phys.subr.edu

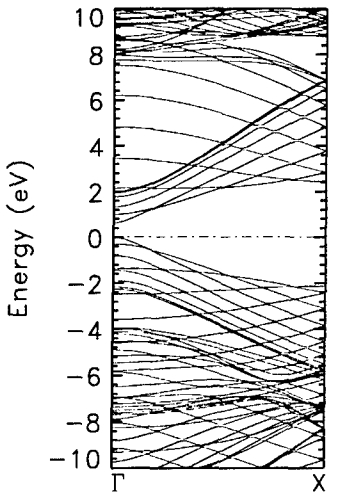

FIG. 1. The electron energy bands of SWCNT (16, 0).

and Kohn-Sham.[15–19] The many-body exchange and correlation interactions of the electron gas are described by the density functional potential in a local density approximation (LDA). We used the Ceperley-Alder form of the exchange-correlation potential.[20] As we reported in the previous publications on the calculations of the electronic structure of SWCNTs,[16] we also performed *ab initio* calculations using the generalized gradient approximation (GGA) potential of Perdew and Yue.[21] We compared the electron energy bands of the SWCNTs from the LDA and GGA calculations. The average difference between the energy bands, resulting from the two potentials, was about 1 mRy. We utilized the LCAO method in solving the Kohn-Sham equations.[22,23] We employed an extended basis set that includes atomic orbitals of C($1s2s3s\ 2p3p$). Here C($3s\ 3p$) are the extra orbitals that are used to augment the basis set to account for possible charge diffusion and polarization in the CNTMs. The real space approach of the LCAO method enables us to complete the required large-scale computations using our Silicon-Graphics Origin2000 that is equipped with 2 GB random access memory (RAM).

As identified in the experimental studies, single-walled carbon nanotubes are self-assembled in a triangular lattice in bundles, strands, or mats. We constructed the carbon nanotube mats by aligning the SWCNTs in an array of the triangular lattice. We vary the distances between the SWCNTs to simulate the different samples of the interactions in the mats. We performed *ab initio* density functional calculations to study the electronic structure of the aligned carbon nanotube mats. We also carried out *ab initio* total energy calculations for the carbon nanotube mats at various tube-tube distances.

For the studies of the optical properties of the aligned CNTMs for photonic applications, we are particularly interested in the semiconducting SWCNTs. We utilized the calculated electronic energy levels and related wave functions to evaluate the dielectric function of the aligned CNTMs. We calculated the real and imaginary parts of the dielectric function of CNTMs as functions of photon energies. The imaginary part of the dielectric function $\varepsilon_2(\omega)$, from the direct interband transitions, is calculated from the Kubo-Greenwood formula,[24]

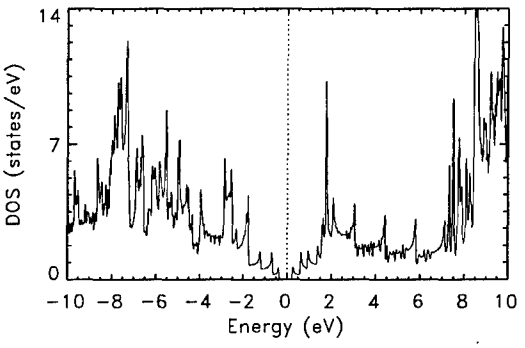

FIG. 2. The electron density of states of SWCNT (16, 0).

$$\varepsilon_2(\omega) = \frac{8\pi^2 e^2}{3m_e^2\hbar\omega^2\Omega}\sum_{\mathbf{k}}\sum_{nl}|\langle\Psi_{\mathbf{k}n}(\mathbf{r})|\mathbf{P}|\Psi_{\mathbf{k}l}(\mathbf{r})\rangle|^2 f_{\mathbf{k}l}(1-f_{\mathbf{k}n}) \times \delta(\varepsilon_{\mathbf{k}n}-\varepsilon_{\mathbf{k}l}-\hbar\omega), \quad (1)$$

where $\hbar\omega$ is the photon energy; $\mathbf{P}$ is the momentum operator, $\mathbf{P}=-i\hbar\nabla$; $\varepsilon_{\mathbf{k}l}$ and $\Psi_{\mathbf{k}l}$ are the eigenenergy and related eigenwave function of the lth state at $\mathbf{k}$ point in the Brillouin zone; $f_{\mathbf{k}l}$ is the Fermi distribution function; and Ω is the volume of the triangular lattice unit cell. The real part of the dielectric function $\varepsilon_1(\omega)$ was found from the well-known Kramers-Kronig (K-K) relation.

III. RESULTS

A. Single-walled carbon nanotube (16, 0) mat

We constructed the carbon nanotube mat utilizing SWCNT (16, 0) as the basic building block. The diameter of individual SWCNT (16, 0) is 1.25 nm, which is comparable to the ones that were experimentally studied by Kazaoui *et al.*[25]

We calculated the electronic structure of individual SWCNT (16, 0). There are 64 atoms in the tube unit cell of SWCNT (16, 0). The large number of atoms per unit cell that enter into the *ab initio* calculations presents some technical challenges. We utilized a real space approach of LCAO calculations. The calculated electron energy bands of SWCNT (16, 0) are presented in Fig. 1, where $\Gamma=(0,0,0)$, $Z=\pi/T(0,0,1)$, and T is the length of the tube unit cell. Figure 1 shows a direct band gap of 0.62 eV at the Γ point. The calculated density of states (DOS) of SWCNT (16, 0) is shown in Fig. 2. The van Hove singularities at the band edges and the sharp structures in the density of states are attributed to the one-dimensional (1D) tube structure.

Subsequently, we calculated the electronic structure of the carbon nanotube mat. In contrast to the work of Guo *et al.*,[11] we aligned the SWCNTs (16, 0) in a triangular lattice to form the mat. Guo *et al.* used a supercell geometry, and the nanotubes were aligned in a square array with the closest distance between the adjacent nanotubes being at least 6 Å. In this work, we performed the *ab initio* total energy calculations for the carbon nanotube mats at various tube-tube distances. The total energy minimization found the stable tube-tube distance at 3.5 Å, which is close to the interplanar distance (3.35 Å) of graphite.

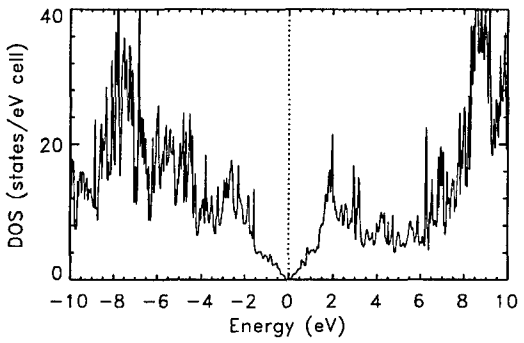

FIG. 3. The electron density of states of carbon nanotube (16, 0) mat at the tube-tube distance of 3.5 Å.

In Fig. 3, we present the electron density of states of the carbon nanotube mat, which was constructed from SWCNTs (16, 0) and the tube-tube distance was at 3.5 Å. The density of states of the CNTM in Fig. 3 retained the van Hove singularities. The weak interaction between the nanotubes slightly smeared the sharp peak structures in the DOS as compared to those of SWCNTs in Fig. 2.

Utilizing the electron energy levels and related wave functions from the electronic structure computations, we further calculated the optical properties of the carbon nanotube mat. We calculated the imaginary (ε_2) part of the dielectric function as a function of photon energy. The real part of the dielectric function $\varepsilon_1(\omega)$ was found from the K-K relation. The calculated dielectric function revealed a strong anisotropy when the electric field (E) of the light is parallel or perpendicular to the tube axis. We present, in Fig. 4, the

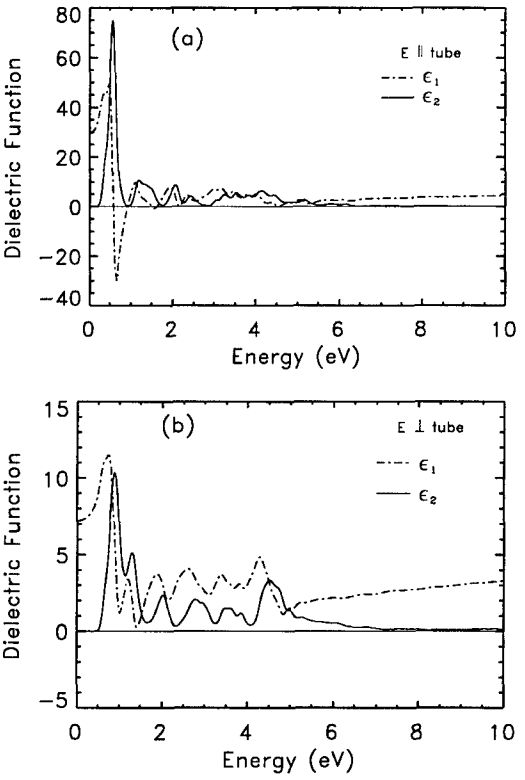

FIG. 4. The calculated real and imaginary parts of the dielectric function, $\varepsilon(\omega)=\varepsilon_1(\omega)+i\varepsilon_2(\omega)$, of the carbon nanotube (16, 0) mat which has the tube-tube distance of 3.5 Å between the SWCNTs (16, 0).

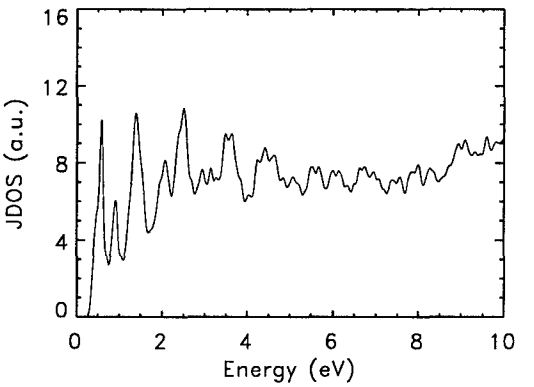

FIG. 5. The joint density of states for the aligned carbon nanotube (16, 0) mat.

calculated dielectric function of the aligned nanotube mat, for the tube-tube distance of 3.5 Å between the individual SWCNTs (16, 0). Figures 4(a) and 4(b) present the dielectric functions ($\varepsilon_1, \varepsilon_2$) for the electric field of the light parallel and perpendicular to the tube axis, respectively. When the electric field of the light is parallel to the tube axis, the imaginary part of the dielectric function ε_2 has a strong peak at the photon energy of about 0.58 eV, as in Fig. 4(a). The height of the first peak of ε_2 in Fig. 4(a) can reach a value of about 60, which is about a factor of 7 higher than that of the first peak of ε_2 (at 0.9 eV) in Fig. 4(b). The strong peak in ε_2 in the low photon energy region in Fig. 4(a) shows a strong anisotropy in the optical properties of CNTM and is spectacularly different from that of conventional optical materials. The above strong peak in ε_2 indicates that the carbon nanotube mats can be used as photonic sensors in the infrared region. Such unusual optical properties in semiconducting carbon nanotube mats present an opportunity for applications in electro-optical devices.

We further studied the physical factors for the strong anisotropy in the optical properties of the aligned carbon nanotube mat. Particularly, a strong anisotropy is observed in the first peaks of the imaginary parts of the dielectric function when the polarization of the light is parallel or perpendicular to the tube axis. It is noted that the first absorption peak in ε_2, in the aligned CNTM, is associated with the van Hove singularities that are located just above and below the Fermi level. We calculated a joint density of states (JDOS) that is based on the same calculation formula as that of the computation of ε_2, but without the inclusion of the electron excitation matrix elements in the calculation. The calculated JDOS of the aligned carbon nanotube (16, 0) mat is shown in Fig. 5. The first peak of the JDOS in Fig. 5, at 0.58 eV, is associated with the first peak of ε_2 in Fig. 4(a) when the electric field of the light is parallel to the tube axis. The second peak of the JDOS in Fig. 5, at about 0.9 eV, is associated with the first peak of ε_2 in Fig. 4(b) when the electric field of the light is perpendicular to the tube axis. The height of the first peak of the JDOS in Fig. 5 is greater than that of the second peak, with a ratio of 1.67. The electron excitation matrix elements that contribute to the first peak of ε_2 in Fig. 4(a) have a much higher value than those contributing to the first peak of ε_2 in Fig. 4(b). The ratio of the excitation matrix

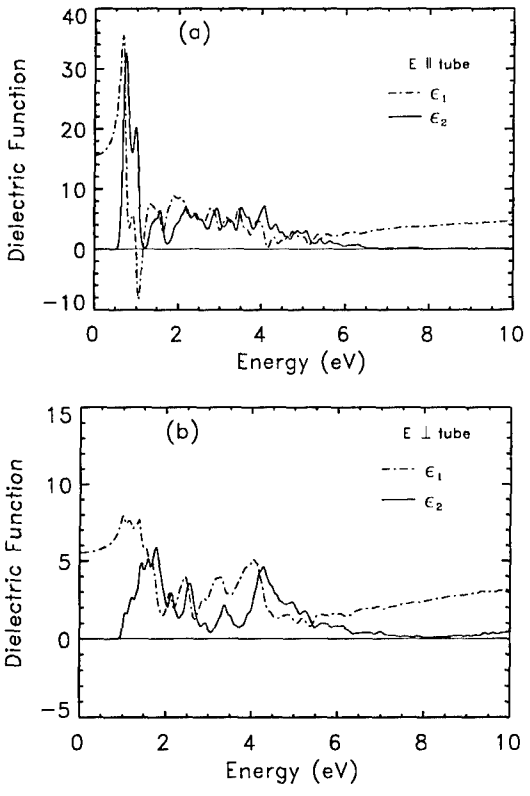

FIG. 6. The calculated real and imaginary parts of the dielectric function of the carbon nanotube (10, 0) mat which has the tube-tube distance of 3.34 Å between the individual SWCNTs (10, 0).

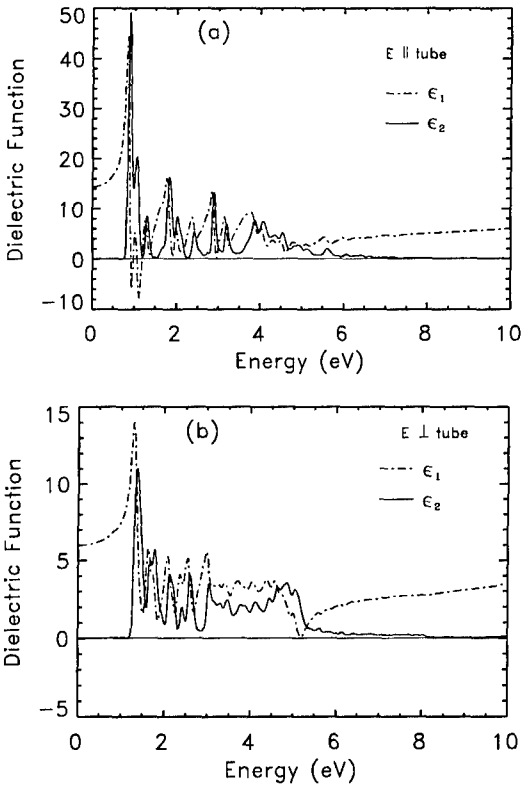

FIG. 7. The calculated real and imaginary parts of the dielectric function of the carbon nanotube (8,4) mat which has the tube-tube distance of 3.34 Å between the chiral SWCNTs (8, 4).

elements accounting for these two peaks is about 4–5. Hence, the strong anisotropy in ε_2 is mainly attributed to the electron excitation matrix elements when the polarization of the light is in different directions.

B. Single-walled carbon nanotube (10, 0) mat

The electronic structure of individual SWCNT (10, 0), from *ab initio* density functional calculations, was presented in previous publications.[16,26] The diameter of individual SWCNT (10, 0) is 7.83 Å. In this work, we calculated the optical properties of the aligned carbon nanotube (10, 0) mat for electro-optical device applications. The SWCNTs (10, 0) are arranged in a triangular lattice in the aligned CNTM. We performed *ab initio* electronic structure calculations for the aligned carbon nanotube (10, 0) mats. We employed the *ab initio* total energy minimization that found a stable tube-tube distance at 3.34 Å. In Fig. 6, we present the calculated real and imaginary parts of the dielectric function of the carbon nanotube (10, 0) mat, for the tube-tube distance of 3.34 Å. The general feature of the dielectric function of the aligned carbon nanotube (10, 0) mat is similar to that of the (16, 0) mat. The calculated imaginary parts of the dielectric function in Fig. 6(a), for the electric field of the light parallel to the tube axis, shows a strong peak near the absorption edge at about 0.75 eV. When the electric field of the light is perpendicular to the tube axis, the absorption is much weaker, as shown in Fig. 6(b). This feature again presents a strong anisotropy in the optical properties of the aligned carbon nanotube (10, 0) mat. The height of the first peak in ε_2 in Fig. 6(a) for the carbon nanotube (10, 0) mat is lower than that of the carbon nanotube (16, 0) mat, which could indicate the effect of the nanotube curvature on the optical properties.

The calculated, strong anisotropy in the optical properties of the aligned carbon nanotube (10, 0) mat as well as the locations of the major absorption peaks in the imaginary part of the dielectric function ε_2 agree with those properties of the isolated or nearly isolated carbon nanotubes that were calculated by Guo *et al.* using supercells of a square array.[11] In this work, we are particularly interested in the aligned carbon nanotube mats that are constructed from semiconducting SWCNTs for optoelectronic applications. Guo *et al.* presented the calculated results of ε_1 and ε_2 for the isolated SWCNT (10, 0) (Fig. 8 in their article)[11] when the electric field is parallel and perpendicular to the nanotube axis. However, they did not present the magnitude of the first absorption peak in ε_2 when the electric field is parallel to the nanotube axis. The location of the first major peak in ε_2 for the electric field in parallel to the nanotube axis was found at about 0.75 eV from our calculation. This finding is in agreement with the result of Guo *et al.* of about 0.8 eV, estimated from their graph.

C. Single-walled carbon nanotube (8, 4) mat

The electronic structure of nonsymmorphic SWCNT (8, 4) has been studied by *ab initio* density functional calculations in previous work.[16,26] The diameter of SWCNT (8, 4) is 8.29 Å. We constructed a carbon nanotube (8, 4) mat by arranging the SWCNTs (8, 4) in a triangular lattice. The tube-tube distance in the mat in the triangular lattice is 3.34 Å, as that in the carbon nanotube (10, 0) mat. We per-

formed *ab initio* density functional computations to study the optical properties of the carbon nanotube (8, 4) mat. Figure 7 presents the calculated optical properties, i.e., the real and imaginary parts of the dielectric functions as functions of the photon energy. Figures 7(a) and 7(b) present the cases of the electric field polarization of the light parallel and perpendicular to the tube axis, respectively. Similar to the carbon nanotube (16, 0) and (10, 0) mats, there is a strong peak in the imaginary part (ε_2) of the dielectric function near the absorption edge at about 0.89 eV, when the electric field of the light is parallel to the tube axis. The imaginary part (ε_2) of the dielectric function can reach a value of about 49 at the photon energy of 0.89 eV. There is a strong anisotropy in the optical properties in the carbon nanotube (8, 4) mat, as shown in Figs. 7(a) and 7(b).

IV. CONCLUSION

In this work, we studied the optical properties of the aligned carbon nanotube (16, 0), (10, 0), and (8, 4) mats for photonic device applications. We employed *ab initio* density functional computations to calculate the imaginary and real parts of the dielectric functions as functions of the photon energy. The calculated dielectric functions of the aligned carbon nanotube (16, 0), (10, 0), and (8, 4) mats present a strong anisotropy when the electric field of the light is parallel or perpendicular to the tube axes. Especially, there are strong peaks in the imaginary part of the dielectric function near the absorption edges, when the electric field of the light is parallel to the carbon nanotube axes. The unusual optical properties of the semiconducting carbon nanotube mats present an opportunity for applications in electro-optical devices in the infrared energy region.

ACKNOWLEDGMENTS

This work was funded in part by the Department of Navy, Office of Naval Research (Grant No. N00014-05-1-0009), by NASA (Award Nos. NCC 2-1344 and NAG 5-10253), and by the National Science Foundation (Award No. 0508245).

[1]Z. Wu *et al.*, Science **305**, 1273 (2004).
[2]Y. Kim, N. Minamia, and S. Kazaoui, Appl. Phys. Lett. **86**, 073103 (2005).
[3]Z. M. Li *et al.*, Phys. Rev. Lett. **87**, 127401 (2001).
[4]L. Vivien *et al.*, Opt. Commun. **174**, 271 (2000).
[5]P. Chen, X. Wu, X. Sun, J. Lin, W. Ji, and K. L. Tan, Phys. Rev. Lett. **82**, 2548 (1999).
[6]W. A. de Heer, W. S. Bacsa, A. Chatelain, T. Gerfin, R. Humphrey-Baker, L. Forro, and D. Ugarte, Science **268**, 845 (1995).
[7]D. E. Milkie, C. Staii, S. Paulson, E. Hindman, A. T. Johnson, and J. M. Kikkawa, Nano Lett. **5**, 1135 (2005).
[8]P. W. Barone, S. Baik, D. A. Heller, and M. S. Strano, Nat. Mater. **4**, 86 (2005).
[9]N. Kouklin, M. Tzolov, D. Straus, A. Yin, and J. M. Xu, Appl. Phys. Lett. **85**, 4463 (2004).
[10]M. S. Dresselhaus, G. Dresselhaus, and A. Jorio, Annu. Rev. Mater. Res. **34**, 247 (2004).
[11]G. Y. Guo, K. C. Chu, D. S. Wang, and C. G. Duan, Phys. Rev. B **69**, 205416 (2004).
[12]M. Machon, S. Reich, C. Thomsen, D. Sanchez-Portal, and P. Ordejon, Phys. Rev. B **66**, 155410 (2002).
[13]H. W. Zhu, C. L. Xu, D. H. Wu, B. Q. Wei, R. Vajtai, and P. M. Ajayan, Science **296**, 884 (2002).
[14]H. Zhu, G. L. Zhao, C. Masarapu, D. P. Young, and B. Wei, Appl. Phys. Lett. **86**, 203107 (2005).
[15]P. Hohenberg and W. Kohn, Phys. Rev. **136**, B864 (1964); W. Kohn and L. J. Sham, Phys. Rev. **140**, A1133 (1965).
[16]G. L. Zhao, D. Bagayoko, and L. Yang, Phys. Rev. B **69**, 245416 (2004).
[17]J. Callaway and N. H. March, *Solid State Physics*, edited by H. Ehrenreich, D. Turnbull, and D. Seitz (Academic, New York, 1984), Vol. 38, p. 135.
[18]G. L. Zhao, D. Bagayoko, and E. G. Wang, Mod. Phys. Lett. B **17**, 375 (2003).
[19]D. Bagayoko, G. L. Zhao, J. D. Fan, and J. T. Wang, J. Phys.: Condens. Matter **10**, 5645 (1998).
[20]S. H. Vosko, L. Wilk, and M. Nusair, Can. J. Phys. **58**, 1200 (1980).
[21]J. P. Perdew and W. Yue, Phys. Rev. B **33**, 8800 (1986); J. P. Perdew, Phys. Rev. B **33**, 8822 (1986); J. P. Perdew and A. Zunger, Phys. Rev. B **23**, 5048 (1981).
[22]S. G. Mikhlin, *The Numerical Performance of Variational Methods* (Wolters-Noordhoff, Groningen, The Netherlands, 1971), Chaps. 1, 2, and 7.
[23]S. H. Gould, *Variational Methods for Eigenvalue Problems* (University of Toronto Press, Toronto, 1957), Chap. 2.
[24]W. Y. Ching, J. Am. Ceram. Soc. **73**, 3135 (1990).
[25]S. Kazaoui, N. Minami, R. Jacquemin, H. Kataura, and Y. Achiba, Phys. Rev. B **60**, 13339 (1999).
[26]A. Pullen, G. L. Zhao, D. Bagayoko, and L. Yang, Phys. Rev. B **71**, 205410 (2005).

Density functional band gaps of AlAs

H. Jin, G. L. Zhao, and D. Bagayoko*
Department of Physics, Southern University and A & M College, Baton Rouge, Louisiana 70813, USA
(Received 13 February 2006; revised manuscript received 27 March 2006; published 27 June 2006)

We present results of *ab initio*, self-consistent calculations of electronic properties of AlAs in the zinc-blende structure. Our nonrelativistic calculations employed the generalized gradient approximation of density functional potential and Bagayoko, Zhao, and Williams implementation method of the linear combination of atomic orbitals formalism. Our calculated indirect band gaps at the X and L points are 2.15 and 2.38 eV, respectively, in good agreement with experimental values. The calculated direct gap at Γ is 25% smaller than the experimental one. We also present calculated total and partial densities of states and the electron effective mass at the bottom of the conduction band at Γ.

DOI: 10.1103/PhysRevB.73.245214 PACS number(s): 71.15.Ap, 71.20.−b, 71.22.+i

I. INTRODUCTION

AlAs has attracted much attention because it is not only one of the most important electronic and optoelectronic materials, but also a very essential component in GaAs-based heterostructures, supperlattices, and quantum wells. There are numerous device applications of $Al_xGa_{1-x}As$ alloys, including diode lasers, light-emitting diodes, photodetectors, and electro-optic modulators. AlAs and its heterostructures have been studied extensively for both their scientific and technological relevance.[1–7]

The theoretical prediction of band structures, fundamental energy gaps, and effective masses of semiconductors and alloys is of great importance for the fabrication of the heterostructures and devices. Over the past 2 decades, there have been many theoretical calculations of the electronic structures of AlAs.[3,5,7–19] To our knowledge, however, except for the fitting approaches such as the tight-binding model,[13,14,16] almost all of the theoretical calculations of the band structure of AlAs led to band gaps that deviate from the experimental values[3,7–12] to varying degrees. Table I lists the referenced theoretical and experimental band gaps of AlAs. For the theoretical works, the table also shows the applicable potential and computational method. Unlike other III-V compounds, AlAs is an indirect band gap semiconductor with the conduction band minimum close to or at the X point[7–12,19] while the valence band maximum is at the gamma (Γ) point. Usually, three band gaps are reported for the AlAs system: the minimum indirect band gap E_g^X, the direct gap E_g^Γ, and the second and larger indirect gap E_g^L. As can be seen from Table I, previous, *ab initio* local density approximation (LDA) calculations typically reported values of the minimum, indirect gap that are 36% to 47% off the measured one.[4] Although the agreement with experiment has been improved dramatically by using the Green function and screened Coulomb potential approximation and the pseudopotential method (GW-PP),[15] the Green function and screened Coulomb potential approximation and the quasiparticle approach (GW-QP),[9] and a semi-*ab initio* approach utilizing a minimum basis set of orthogonalized functions in a linear combination of atomic orbitals (OLCAO)[8] and an additional atomiclike potential, the discrepancies for the calculated band gaps E_g^X, E_g^Γ, and E_g^L have remained significant. These band gaps, for the GW-PP[15] and the GW-QP are 2.08, 2.75, and 2.79 eV for the former and 2.09, 3.26, and 2.81 for the latter. While the improvement for the minimum, indirect gap is significant, the overestimations of the larger, indirect gap are by 18% and 28% for the GW-PP and GW-QP calculations, respectively.

The above discrepancies are key motivations for this work that employs a GGA potential and the Bagayoko, Zhao and Williams (BZW) method[20,21] within the linear combination of atomic orbital formalism (LCAO). The BZW method has been successfully applied to reproduce or to predict the band gaps of numerous semiconductors, including cubic InN,[22] wurtzite InN,[23] GaN, Si, and C,[21] and carbon nanotubes.[24,25]

II. COMPUTATIONAL METHOD AND DETAILS

Our nonrelativistic calculations employed a nonlocal density functional potential from the generalized gradient approximation (GGA).[26–28] We utilized the formalism of the linear combination of atomic orbitals (LCAO) in real space. The implementation of the BZW method in carrying out the self-consistent computations is the major, distinctive feature of the present work as compared to previous works on AlAs. The details of the BZW procedure are widely available in the literature[21–25] and are discussed further below. A brief overview of its implementation follows.

In the implementation of the BZW procedure, we started the self-consistent calculations with a minimal basis set, i.e., the basis set just accounting for all the electrons in the atomic or ionic species present in the system under study. For AlAs, we chose the ions Al^{1+} and As^{1-} for our self-consistent calculations, as preliminary studies indicated charge transfers closer to these species, i.e., the self-consistent system is approximately $Al^{0.94+}As^{0.94-}$. We subsequently carried out several other self-consistent calculations with larger and larger basis sets by augmenting with one or more ionic orbitals that belong to the next and lowest-lying energy levels in Al^{1+} or As^{1-}. The occupied bands of a given calculation are compared to those of the previous one until they are found to be identical in numerical values, curvature, and branching, within computational uncertainties. The results reported here are those of the calculation before the last one. The basis set for this calculation (i.e., VII for AlAs) is referred to as the optimal basis set. As explained further be-

TABLE I. Comparison of theoretical and experimental band gaps of zinc-blende AlAs. The three band gaps at respective $\Gamma_{15v}-X_{1c}$, $\Gamma_{15v}-\Gamma_{1c}$, and $\Gamma_{15v}-L_{1c}$.

Potential	Computational method	E_g^X (eV)	E_g^Γ (eV)	E_g^L (eV)
Experiment 1	Photoluminescence (T=12 K)	2.25[a]		
Experiment 2	Excitonic gap, photoluminescence (T=4 K)	2.23[b]	3.13[b]	
	Excitonic gap, photoluminescence (T=300 K)	2.15[b]	3.03[b]	
Experiment 3	Transport (T=295 K)	2.16[c]	2.98[c]	2.36[c]
GGA	LCAO-BZW (Present work) a=5.66 Å	2.15	2.35	2.38
GGA	LCAO-BZW (Present work) a=5.6524 Å	2.14	2.38	2.39
LDA	Projector-augmented-wave (PAW)	1.32[d]	1.94[d]	2.06[d]
GW	PAW	1.57[d]	2.7[d]	2.73 [d]
LDA	Pseudopotential method (PP)	1.20[e]	1.77[e]	1.89[e]
GW	PP	2.08[e]	2.75[e]	2.79[e]
LDA	*Ab initio* PP	1.44[f]	2.35[f]	2.12[f]
LDF	First-principles full-potential self-consistent linearized-muffin-tin-orbital (LMTO)	1.31[g]		
	Ab-initio PP	1.3[h]	2.5[h]	
LDA	Self-consistent full-potential linearized-augmented-plane-wave (FLAPW)	1.36[i]	1.95[i]	2.07[i]
GW	Quasiparticle (QP)	2.09[j]	3.26[j]	3.03[j]
LDF	Minimal basis semi-*ab initio* orthogonalized LCAO method	2.37[k]	2.79[k]	2.81[k]
Tight-binding model (TBM)	PP	2.21[l]	2.79[l]	2.48[l]
TBM		2.142[m]	2.998[m]	2.313[m]
TBM		2.262[n]	2.974[n]	2.756[n]

[a]Reference4.
[b]Reference1.
[c]Reference2.
[d]Reference7.
[e]Reference15.
[f]Reference12.
[g]Reference11.
[h]Reference10.
[i]Reference3.
[j]Reference9.
[k]Reference8.
[l]Reference16.
[m]Reference13.
[n]Reference14.

low in the discussion section, upon the convergence of the charge density, potential, and occupied energy levels, as is the case for the calculation with the optimal basis set, computations with larger basis set are inherently affected by a basis set and variational effect. This effect stems from the use of a variational approach where the charge density is computed using only the wave functions of occupied states and consequences of the Rayleigh theorem.[21–23] Table II shows the basis sets employed in the various, self-consistent calculations we performed for AlAs. The results discussed here are those from Calculation VII for which the basis set is optimal in the sense specified above.

We utilized an expanded version of the electronic structure calculation program package from the Ames Laboratory of the Department of Energy (DOE).[29–31] AlAs, in the zinc-blende structure, is a member of the III-V family and belongs to the T_d^2–$F\bar{4}3m$ space group. As per Table I, only Experiment 3, done at a temperature of 295 K, provides[2] values for the two indirect and one direct gaps noted above. For comparison purposes, we selected the experimental lattice parameter of a=5.66 Å for a temperature of 291 K.[34] Except for the gap values shown in Table I for a zero-temperature lattice constant[6] of 5.6524 Å, the results discussed here are for the above room temperature lattice constant. The atomic wave

TABLE II. The atomic orbitals used in calculations I to VIII for AlAs. Superscript zeros indicate added orbitals representing unoccupied atomic states.

Basis set 0: core-state orbitals in calculations I to VIII: Al (1s), As (1s,2s,2p)
Basis set I: Al(1s,2s,2p,3s), As(1s,2s,2p,3s,3p,3d,4s,4p)
Basis set II: Set I plus Al($3p^0$)
Basis set III: Set II plus As($5s^0$)
Basis set IV: Set III plus Al($4s^0$)
Basis set V: Set IV plus As($4d^0$)
Basis set VI: Set V plus Al($3d^0$)
Basis set VII: Set VI plus As($5p^0$)
Basis set VIII: Set VII plus Al($4p^0$)

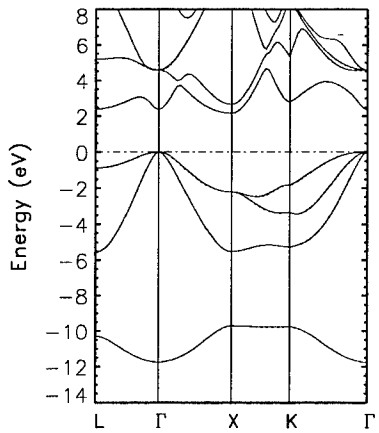

FIG. 1. Electronic band structure of AlAs. The solid lines represent the results from Calculation VII and the dashed lines those from Calculation VIII. Other results in Tables I and III and Figs. 2 and 3 are from Calculation VII. The lattice constant is 5.66 Å.

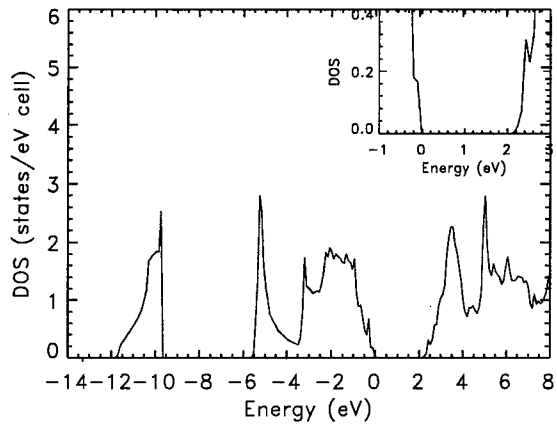

FIG. 2. The calculated density of states for AlAs, as obtained from the bands from Calculation VII, for a lattice constant of 5.66 Å. The inset shows the practically measurable band gap from 2.14 to 2.4 eV.

functions of the ionic states of Al^{1+} and As^{1-} were obtained from self-consistent, *ab initio*, atomic calculations. The radial parts of the atomic wave functions were expanded in terms of Gaussian functions. Sets of even-tempered Gaussian exponentials were employed with a minimum of 0.10 for both Al and As, and a maximum of 4.5000×10^4 for Al and 1.5000×10^5 for As, in atomic units. We used 19, 19, and 17 orbitals for the s, p, and d states for both Al and As. A mesh of 60 k points, with proper weights in the irreducible Brillouin zone, was employed in the self-consistent iterations. The computational error for the valence charge was about 0.000129 for 34 electrons. The self-consistent potentials converged to a difference of 10^{-5} after about 30 iterations. The total number of iterations varied with the input potentials. The basis sets for each of the self-consistent calculations used in the BZW procedure in this work are listed in Table II. The optimal basis set for the AlAs calculation is the basis set for calculation VII.

III. RESULTS

Figure 1 shows the band structure of AlAs at high symmetry points and along high symmetry lines in the Brillouin zone. The calculated conduction band minimum is at the X point while the valence band maximum is at Γ, in agreement with experiment. The energy levels at high symmetry points in the Brillouin zone are listed in Table III. Our calculated, indirect, fundamental band gap value of 2.15 eV agrees very well with the experimental values of 2.15 and 2.16 eV, at room temperature, and is lower, by less than 5%, than the zero temperature values of 2.23 and 2.25 eV, as shown in Table I. Similarly, the calculated indirect band gap at the L point, 2.38 eV, agrees very well with the experimental finding of 2.36 eV. However, our direct band gap of 2.35 eV is about 21% and 25% lower than the measured values, as discussed further below.

TABLE III. Electronic energies (eV) at high symmetry points, with the top of the valence band set to 0 eV. Data are from Calculation VII for a lattice constant of 5.66 Å.

Γ	X	L	K
−11.74	−9.70	−10.30	−9.74
0.00	−5.52	−5.56	−5.27
0.00	−2.21	−0.88	−3.33
2.35	2.15	2.38	−1.84
4.58	2.65	5.20	2.79

Figures 2 and 3 show the total (DOS) and partial densities of states (PDOS) for AlAs, respectively, as obtained from Calculation VII. The total DOS curves, particularly the inset, show that the practically measurable band gap could be anywhere between 2.14 and 2.4 eV, where the latter corresponds to a value of 0.1 for the DOS, in excellent agreement with experiments.[1,2,5] The lowest peak between −11.8 and −9.7 eV arises from the Al($3p$) and As($4s$) orbitals. The peaks appearing between −5.6 and 0 eV stem from Al($3s$), Al($3p$), and As($4p$) orbitals. A significant hybridization of

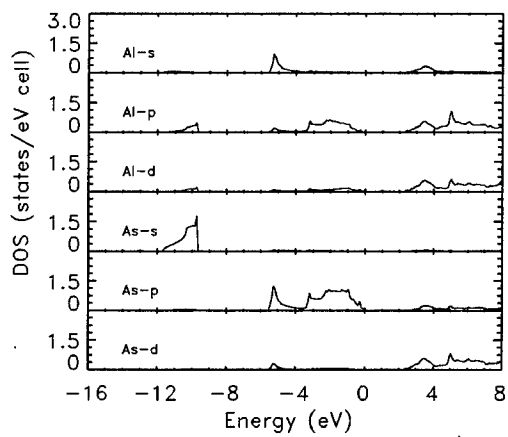

FIG. 3. The partial density of states (PDOS) for AlAs from the contribution of the s, p, and d states of Al and As atoms, respectively. These PDOS are derived from the bands from Calculation VII, for a lattice constant of 5.66 Å.

Al($4p$), Al($3d$), and As($4d$) orbitals is apparent in the PDOS curve in Fig. 3.

Our calculated electron effective mass of AlAs, m^*, at the bottom of the conduction band at the Γ point, is 0.15 m_0, where m_0 is the free-electron mass. This result is also in excellent agreement with the experimental value of 0.15 m_0 in Ref. 32 and is 21% higher than the 0.124 m_0 estimated from a fit to absorption data.[33]

IV. DISCUSSIONS

In comparison to previous density functional and other calculations, this work has resolved most of the discrepancies between experiment and theory. Previous density functional calculations, as per the content of Table I, woefully underestimated the indirect band gaps and the direct one. The GW calculations improved the agreement between theory and experiment for the fundamental, indirect gap, by reducing the underestimation to about 3% from the room temperature value. For the larger indirect gap at L, however, they overestimated significantly (by 18% and 28%). While GW-PP[15] underestimates the room temperature direct gap by close to 8%, the GW-QP[9] overestimates it by 9%. Vurgaftman *et al.*[6] underscored the difficulties associated with the experimental determination of the direct gap at Γ. These difficulties are apparent in the work of Monemar[1] where high impurity concentrations caused a broadening of exciton spectra. Consequently, the well-defined dip in the spectrum, that would have indicated the direct gap, is replaced by a much broader dip from the uncertain location of which one extracts the value of the direct gap. We expect the uncertainties associated with the determination of this direct gap to contribute to the unusual deviation of our calculated value from experiment. Further, given that this gap is not the minimum one, GGA-BZW calculations are not necessarily expected to describe it correctly from a ground state theory as it does for the fundamental bang gap.[20–25]

A central issue in these discussions relates to the physical and mathematical reasons that explain the success of the BZW method where many others have failed, including some rather sophisticated approaches that go beyond density functional theory. The answer resides in a thorough understanding of basis set related effects on the outcomes of these calculations. Specifically, as discussed by Bagayoko et al,[35] LCAO type calculations have to ascertain the completeness of the basis set. In doing so, one typically includes diffuse orbitals, with relatively small exponents, to accommodate the charge redistribution in the molecular or solid state environments as compared to those for atoms or ions. Additionally, one has to provide for angular symmetries that may arise in molecular or solid environments. Most works cited herein appear to have handled these two points correctly.

There is still a nontrivial basis set related effect distinct from the issues of angular symmetry and of diffuse orbitals. The preoccupation for guaranteeing the completeness of the basis set explains the use of as large basis sets as possible, as long as linear dependency is avoided. Consequently, no particular limit is placed on the size of the basis set. This size often varies widely from one group of investigators to another, even for the same system and for similar orbitals (i.e., Gaussians). The Rayleigh theorem,[36,37] however, indicates that serious problems could be associated with arbitrarily large basis sets. The statement of this rigorous, mathematical theorem follows: *Let an eigenvalue equation be solved twice, by an LCAO method, respectively, with N and (N+1) orbitals—such that the (N+1) orbitals of Calculation II include all the N orbitals of Calculation I plus an additional one—and let the eigenvalues from the two calculations be ordered from the lowest (ε_1^N and $\varepsilon_1^{(N+1)}$ for I and II, respectively) to the highest (ε_N^N and $\varepsilon_{(N+1)}^{(N+1)}$, respectively), then the theorem states that $\varepsilon_i^{(N+1)} \leq \varepsilon_i^N$ for all $i \leq N$.* Alternatively, this theorem states that a variational eigenvalue, upon an increase of the basis set (and hence of the dimension of the matrix), is not increased. It either stays the same (if it is equal to the exact, physical eigenvalue of the matrix) or it decreases to approach this exact eigenvalue from above. This theorem therefore points to the need to utilize as large a basis set as possible in order to lower variational eigenvalues to reach the exact ones. Such a large basis set is also needed to ensure completeness. Bagayoko, Zhao, and Williams[20,21] identified a basis set and variational effect stemming from any lowering of unoccupied energy levels or bands, for molecules or solids, respectively, when the occupied levels or bands have converged (vis-à-vis an increase of the basis set). The effect can exist in any variational calculations for which the occupied and unoccupied states are not treated in identical manners. Specifically, for all variational calculations of which we know, the occupied and unoccupied states are treated in fundamentally different manners: in the iterative process toward self-consistency, the charge density is constructed or reconstructed *using only the wave functions of the occupied states*. Hence, only the wave functions of these states affect the charge density, the potential, and the Hamiltonian itself, i.e., the physics of the system. It is therefore necessary to guarantee that an applicable basis set is large enough to ensure the convergence of the occupied levels or bands vis-à-vis the size of the basis set. To do so, Bagayoko, Zhao, and Williams (BZW) introduced their method that requires the utilization of a minimum basis set for the first, self-consistent calculation. The outcomes of this first calculation are generally not the correct solutions for the physical system under study. The method therefore requires subsequent calculations where the basis set is methodically augmented as described above and elsewhere.[20,21] The *occupied* energy levels or bands of a calculation are compared to those of the previous one that has a smaller basis set. This process continues until calculation N and $(N+1)$ have the same occupied energy levels or bands, within applicable uncertainties. We then select the outputs of calculation N as the physical description of the system. Indeed, in light of the Rayleigh theorem, some unoccupied energy levels or bands of Calculation $(N+1)$ are generally lower as compared to their counterpart from Calculation N. The BZW method ascribes any such additional lowering of an unoccupied band, while the occupied ones do not change, to mathematical artifacts stemming directly from the Rayleigh theorem. While the method applies to all variational calculations of the Rayleigh-Ritz type that employ an LCAO approach, it is particularly perti-

nent for density functional calculations. Indeed, density functional theory is fundamentally a ground state theory. The BZW method verifiably guarantees the proper description of the ground state with a basis that is sufficiently large. Variational calculations that do not employ the method generally have large enough basis sets to describe the applicable system. However, they do not actually verify that the size of the basis set converged vis-à-vis the description of the occupied states and they do not avoid Rayleigh-theorem related lowering of some unoccupied levels or bands on purely mathematical ground—given that the Hamiltonian (i.e., the physics) does not change once the optimal basis size of the BZW method is attained.

V. CONCLUSION

In conclusion, we successfully performed *ab initio*, self-consistent GGA-BZW calculations for the band structure of a zinc-blende AlAs semiconductor. Our calculated band gaps, except for the direct gap at Γ, are in excellent agreement with measured values. Our calculated effective mass also agrees very well with a directly determined experimental value and disagrees with an estimate derived from fitting to absorption data.

ACKNOWLEDGMENTS

This work was funded in part by the Department of the Navy, Office of Naval Research (ONR, Grant No. N00014-05-1-0009), NASA (Award Nos. NCC 2-1344 and NAG 5-10253), and by the National Science Foundation (Award No. HRD 0000272). The authors are indebted to S. Hasan for his excellent technical support with the computing facilities.

*Corresponding author. Email address: bagayoko@phys.subr.edu or babayoko@aol.com

[1] B. Monemar, Phys. Rev. B **8**, 5711 (1973).
[2] H. J. Lee, L. Y. Juravel, J. C. Woolley, and A. J. Spring Thorpe, Phys. Rev. B **21**, 659 (1980).
[3] B. I. Min, S. Massidda, and A. J. Freeman, Phys. Rev. B **38**, 1970 (1988).
[4] M. Guzzi, E. Grilli, S. Oggioni, J. L. Staehli, C. Bosio, and L. Pavesi, Phys. Rev. B **45**, 10951 (1992).
[5] Ming-Zhu Huang and W. Y. Ching, Phys. Rev. B **47**, 9449 (1993).
[6] I. Vurgaftman, J. R. Meyer, and L. R. Ram-Mohan, J. Appl. Phys. **89**, 5815 (2001).
[7] S. Lebegue, B. Arnaud, M. Alouani, and P. E. Bloechl, Phys. Rev. B **67**, 155208 (2003).
[8] Ming-Zhu Huang and W. Y. Ching, J. Phys. Chem. Solids **46**, 977 (1985).
[9] R. W. Godby, M. Schluter, and L. J. Sham, Phys. Rev. B **35**, 4170 (1987).
[10] P. Boguslawski and I. Gorczyca, Acta Phys. Pol. A **80**, 433 (1991).
[11] Bal K. Agrawal and Savitri Agrawal, Phys. Rev. B **45**, 8321 (1992).
[12] Q. Guo, C. K. Ong, H. C. Poon, and Y. P. Feng, Phys. Status Solidi B **197**, 111 (1996).
[13] Timothy B. Boykin, Phys. Rev. B **54**, 8107 (1996).
[14] J. P. Loehr and D. N. Talwar, Phys. Rev. B **55**, 4353 (1997).
[15] E. L. Shirley, X. Zhu, and S. G. Louie, Phys. Rev. B **56**, 6648 (1997).
[16] An-Ban Chen and Arden Sher, Phys. Rev. B **22**, 3886 (1980).
[17] K. A. Mader and A. Zunger, Phys. Rev. B **50**, 17393 (1994).
[18] E. Hess, I. Topol, K.-R. Schulze, H. Neumann, and K. Unger, Phys. Status Solidi B **55**, 187 (1973).
[19] J. J. Finley, R. J. Teissier, M. S. Skolnick, J. W. Cockburn, G. A. Roberts, R. Grey, G. Hill, M. A. Pate, and R. Planel, Phys. Rev. B **58**, 10619 (1998).
[20] D. Bagayoko, G. L. Zhao, J. D. Fan, and J. T. Wang, J. Phys.: Condens. Matter **10**, 5645 (1998).
[21] G. L. Zhao, D. Bagayoko, and T. D. Williams, Phys. Rev. B **60**, 1563 (1999).
[22] D. Bagayoko, L. Franklin, and G. L. Zhao, J. Appl. Phys. **96**, 4297 (2004).
[23] D. Bagayoko and L. Franklin, J. Appl. Phys. **97**, 123708 (2005).
[24] A. Pullen, G. L. Zhao, D. Bagayoko, and L. Yang, Phys. Rev. B **71**, 205410 (2005).
[25] G. L. Zhao, D. Bagayoko, and L. Yang, Phys. Rev. B **69**, 245416 (2004).
[26] J. P. Perdew, K. Burke, and Y. Wang, Phys. Rev. B **54**, 16533 (1996); see also Phys. Rev. B **57**, 14999 (1998).
[27] J. P. Perdew and Y. Wang, Phys. Rev. B **33**, 8800 (1986).
[28] J. P. Perdew, Phys. Rev. B **33**, 8822 (1986).
[29] P. J. Feibelman, J. A. Appelbaum, and D. R. Hamann, Phys. Rev. B **20**, 1433 (1979).
[30] B. N. Harmon, W. Weber, and D. R. Hamann, Phys. Rev. B **25**, 1109 (1982).
[31] G. L. Zhao, T. C. Leung, B. N. Harmon, M. Keil, M. Mullner, and W. Weber, Phys. Rev. B **40**, 7999 (1989).
[32] M. Zachau, F. Koch, G. Weimann, and W. Schlapp, Phys. Rev. B **33**, 8564 (1986).
[33] W. P. Dumke, M. R. Lorenz, and G. D. Pettit, Phys. Rev. B **5**, 2978 (1972).
[34] W. B. Pearson, *A Handbook of Lattice Spacing and Structure of Metals and Alloys* (Pergamon Press, Oxford-London, 1967).
[35] D. Bagayoko and Pui-Man Lam at SUBR; Nathan Brener and Joseph Callaway at LSU; Phys. Rev. B **54**, 12184 (1996).
[36] D. Bagayoko, Int. J. Quantum Chem. **17**, 527 (1983).
[37] S. H. Gould, *Variational Methods for Eigenvalue Problems* (University of Toronto Press, Toronto, 1957), Chap. 2.

Structural, elastic, and electronic properties of deformed carbon nanotubes under uniaxial strain

A. Pullen,[1] G. L. Zhao,[1,*] D. Bagayoko,[1] and L. Yang[2]
[1]*Department of Physics, Southern University and A & M College, Baton Rouge, Louisiana 70813, USA*
[2]*Eloret, NASA Ames Research Center, MS230-3, Moffett Field, California 94035, USA*
(Received 7 May 2004; revised manuscript received 20 January 2005; published 25 May 2005)

We report structural, elastic, and electronic properties of selected, deformed, single-wall carbon nanotubes under uniaxial strain. We utilized a generalized gradient approximation potential of density functional theory and the linear combination of atomic orbital formalism. We discuss bond-lengths, tubule radii, and the band gaps as functions of tension and compression strain for carbon nanotubes (10, 0), (8, 4), and (10, 10) which have chiral angles of 0, 19.1, and 30 deg relative to the zigzag direction. We also calculated the Young's modulus and the in-plane stiffness for each of these three nanotubes as representatives of zigzag, chiral, and armchair nanotubes, respectively. We found that these carbon nanotubes have unique structural properties consisting of a strong tendency to retain their tubule radii under large tension and compression strains.

DOI: 10.1103/PhysRevB.71.205410 PACS number(s): 73.22.−f, 61.46.+w

Single-wall carbon nanotubes (SWCNTs) can be viewed as rolled-up graphene sheets that have a diameter at the order of 1 nm. They have properties such as high current density, high elasticity, and stiffness unparalleled by other materials. Their potential applications range from that in building skyscrapers and elevator cables to the ones in very tiny electrical circuits and machines.[1] These materials, however, are too small for many conventional measurements. This situation underscores the possible importance of theoretical studies, including the one reported here that focuses on structural, elastic, and electronic properties of selected single-wall carbon nanotubes under uniaxial strain.

In the last several years, tight-binding calculations have been extensively used to study the structural and electronic structure of carbon nanotubes.[2–6] Tight-binding approximations based on the symmetry of the honeycomb lattice of graphite predicted that SWCNTs could be semiconducting or metallic depending on their chirality (n,m). The tight-binding model has been able to provide good estimates of the basic electronic structure of SWCNTs. However, curvature-related effects and the hybridization of different electronic states of graphite could lead to structural and electronic properties that are substantially different from the result of tight-binding calculations. Zigzag $(n,0)$ (where n is a multiple of 3) SWCNTs which were predicted to be metallic from tight-binding calculations were found to have small energy gaps.[7] Several theoretical groups have studied the elastic properties of carbon nanotubes. Their approaches include simulations with realistic many-body potentials,[8] the empirical force-constant method,[9] tight-binding formalisms,[6,10] pseudopotential calculations with local density approximation potentials,[11] and Born's perturbation technique within a lattice dynamics model.[12]

The aim of this work is therefore to study the aforementioned properties of SWCNTs, utilizing *ab initio* quantum computations. We specifically report on structural, elastic, and electronic properties of SWCNTs under uniaxial strain. Recent tight-binding calculations have led to values of bond lengths and radii, band gaps, and Fermi levels as functions of strain.[6] The dependence of tight-binding results upon the selected parameters partly suggests the present work that employs an *ab initio* approach.

Three main features characterize our first-principles computational method. The first of these features is the choice of the potential. We utilized the generalized gradient approximation (GGA) potential of Perdew and Wang.[13] This density functional[14–16] potential goes beyond the local density approximation (LDA). We also performed LDA calculations for carbon nanotube (10, 0). The second feature of our method stems from employing the linear combination of atomic orbital (LCAO). The third and distinctive feature of our work resides in our use of optimal basis sets as per the Bagayoko, Zhao, and Williams (BZW) procedure.[17–20] As explained elsewhere, this procedure avoids a basis set and variational effect inherently associated with variational calculations that employ a basis set and leads to the calculated band gaps in very good agreement with experiments.[17–20] With the above method, we solved the Kohn-Sham[14,15] equation self-consistently. Self-consistency was followed by the calculations of the total energies. Details of these steps, including the Kohn-Sham equation and the expression for the total energy, are fully described in the literature.[14–20]

In the LCAO method, we expanded the electronic eigenfunction Ψ_{ki} of the many-atom system as a linear combination of atomic wave functions.[17] These input functions result from *ab initio* calculations for atomic species that are present in the system. For the calculations, the C(1s) state was used as the core state. For the (10, 0) and the (8, 4) tubes, the C(2s2p) states were used as filled and partially filled valence states. The C(3s3p) orbitals were the unfilled electron states that were used to augment the basis set for the calculations. For the (10, 10) tube, the C(2s2p) states were used as filled and partially filled valence states and the C(3s) as the unfilled state. The empty C(3p) state was dropped, in the case of (10, 10), due to convergence difficulties.

Uniaxial strain was simulated by linearly scaling the atom positions along the tube axis in the carbon nanotube. To find how the tube radius changes with uniaxial strain, after the tube axis was scaled, the radius was identified from the total energy minimization procedure. Namely, for a given nano-

TABLE II. Coefficients m of linear variation of normalized bond lengths with compression (negative) and tensile (positive) strain (i.e., ε expressed as −0.04 and +0.06 for 4% and 6% compression and tensile strain, respectively). $\Delta l/l_0 = m\varepsilon$, where l is the a, b, or c bond length. The Young's modulus Y is in TPa. The in-plane stiffness C is in J/m^2.

Nanotubes	m for bond a	m for bond b	m for bond c	Y (TPa)	C (J/m^2)
(10,0)	0.252	0.252	1.000	1.47	340
(8,4)	0.036	0.572	0.893	1.10	267
(10,10)	0.746	0.746	0[a]	0.726	272

[a]Bond c, for (10,10), is along the circumference of the tube.

a_0 and b_0 and 1.406 Å for c_0, that is about 1% smaller than the results of the *ab initio* GGA calculations. The *ab initio* LDA calculations for SWCNT (10, 0) also found that the radii of the nanotube did not change under a substantially large uniaxial strain. Among the previous *ab initio* calculations of the elastic properties of carbon nanotubes, Sanchez-Portal *et al.* utilized a minimal basis set of one s and three p orbitals per carbon atom and performed LDA calculations.[24] In their calculations, they used pseudoatomic orbitals.[24] Van Lier *et al.* utilized *ab initio* Hartree-Fock 6-31G method and closed nanotube models in their simulations.[25] Sanchez-Portal *et al.*[24] and Van Lier *et al.*[25] reported relatively small values (from 0.14 to 0.19) of the Poisson ratio for their calculated carbon nanotubes, which also indicated the diameter rigidity of the carbon nanotubes. These previous *ab initio* calculations utilized different computational methods, such as a minimal basis set and the Hartree-Fock method, and their results are slightly different from ours. As demonstrated in one of our previous publications,[30] the use of a minimal basis set may not be sufficient to obtain a highly accurate solution of the calculated electronic structure of the carbon nanotubes, which could explain in part the difference between our results and those of Sanchez-Portal *et al.* The fundamental differences between the Hartree-Fock method and density functional methods, i.e., the inclusion of the electronic correlation effects in the latter, partly explain the difference between our results and those of Van Lier *et al.* In our *ab initio* calculations, we utilized extended atomic basis sets and performed both GGA and LDA computations.

The calculated Young's moduli Y (in TPa) for the tubes are shown in Table II. We recall that the radius included in the formula for the Young's modulus is from the center of the tube to the outer circumference. This value of the radius led to Young's moduli close to the experimentally found value of approximately 1 TPa.[9] The (10, 0) and (10, 10) tubes have the highest and lowest Young's moduli, respectively. This trend is expected due to the bond geometry of the tubes according to chirality. All three bonds in the (10, 0) tube have a significant component parallel to the axis along which strain is applied. In the case of (10, 0), the c bond is entirely along the axis. In contrast, one of the bonds of the (10, 10) tube is entirely along the circumference; it is not expected to oppose any resistance neither to compression nor to tensile strain. For this reason, nanotube (10, 10) is intuitively the easiest to stretch or to compress, as confirmed by our results in Table II.

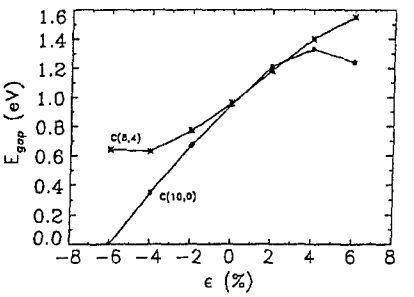

FIG. 3. Band gaps of indicated carbon nanotubes as functions of compression and tensile strain.

We also calculated the in-plane stiffness C for the carbon nanotubes. It is 340, 267, and 272 J/m^2 for (10, 0), (8, 4), and (10, 10), respectively. The in-plane stiffness of these nanotubes exhibited a dependence on their chirality, when the nanotubes are strained along the tube axis (z-direction). Xiao and Liao reported an average in-plane stiffness C of 328 J/m^2 for graphene, using the second-generation Brenner potential in their simulation of carbon nanotubes.[22]

The calculated electronic properties for the unstrained nanotubes basically reproduced the results of Zhao *et al.*[20] for (10, 0) and (8, 4), using the optimal basis sets of the BZW method, which gave converged results for the calculated electronic structure that included the occupied electron states as well as the unoccupied ones near the Fermi level. These tubes were found to be semiconductors. These authors provided plots of the band structures of these tubules.[20] The electron energy bands of carbon nanotube (10, 10) present a semimetallic property as reported in previous publications. Figure 3 shows the nonlinear variation of band gaps of (10, 0) and (8, 4) with strain. For both nanotubes, the band gap decreases with compression strain and increases with tensile strain, for strain values smaller than or equal to 4%. While the band gap for (8, 4) reaches a minimum for a compression strain of 4%, that for (10, 0) exhibits a maximum for a tensile strain of 4%. Our results for the variation of the band gap with strain qualitatively agree with the findings from tight binding[21] but are quantitatively different,[6] particularly in the magnitudes of the band gaps. As apparent in Fig. 3, our results indicate that nanotube (10, 0) become metallic at 6% compression strain. It was noticed that the carbon nanotubes may collapse for large strains,[32,33] a process that we cannot simulate at present using the *ab initio* quantum calculations, because the required computations are beyond our current computation capability. Therefore, the obtained band gaps for large strains may be a theoretical simulation. *A priori*, the general behavior of these band gaps with strain, particularly from values below 4%, is expected on the basis of the increase or decrease of the overlap between atomic sites, for compression or tensile strains, respectively. The consequent broadening or flattening of the bands, respectively, affects the gaps.

A discussion of our results for the elastic properties is partly limited by the dearth of experimental data and by the rather large uncertainty associated with currently available

1563 (1999).
[18] D. Bagayoko, G. L. Zhao, J. D. Fan, and J. T. Wang, J. Phys.: Condens. Matter **10**(25), 5645 (1998).
[19] D. Bagayoko and G. L. Zhao, Int. J. Mod. Phys. B **13**(29, 30 & 31), 3767 (1999).
[20] G. L. Zhao, D. Bagayoko, and L. Yang, Phys. Rev. B **69**, 245416 (2004).
[21] M. Dresselhaus, G. Dresselhaus, and P. Ecklund, *Science of Fullerenes and Carbon Nanotubes* (Academic Press, San Diego, 1996); also see C. Kittel, *Introduction to Solid State Physics*, 7th ed. (Wiley, Brisbane, 1996).
[22] T. Xiao and K. Liao, Phys. Rev. B **66**, 153407 (2002).
[23] A. Sears and R. C. Batra, Phys. Rev. B **69**, 235406 (2004).
[24] D. Sanchez-Portal, E. Artacho, J. M. Soler, A. Rubio, and P. Ordejon, Phys. Rev. B **59**, 12 678 (1999).
[25] G. Van Lier, C. Van Alsenoy, V. Van Doren, and P. Geerlings, Chem. Phys. Lett. **326**, 181 (2000).
[26] M. M. J. Treacy, T. W. Ebbesen, and J. M. Gibson, Nature (London) **381**, 678 (1996).
[27] E. W. Wong, P. E. Sheehan, and C. M. Lieber, Science **277**, 1971 (1997).
[28] Peihong Zhang, Paul E. Lammert, and Vincent H. Crespi, Phys. Rev. Lett. **81**, 5346 (1998).
[29] O. L. Blakslee *et al.*, J. Appl. Phys. **41**, 3373 (1970); E. J. Seldin and C. W. Nezbeda, *ibid.* **41**, 3389 (1970).
[30] S. Reich, C. Thomsen, and P. Ordejón, Phys. Rev. B **65**, 155411 (2002).
[31] E. D. Minot, Yuval Yaish, Vera Sazonova, Ji-Yong Park, Markus Brink, and Paul L. McEuen, Phys. Rev. Lett. **90**(15), 156401 (2003).
[32] S. B. Cronin, A. K. Swan, M. S. Unlu, B. B. Goldberg, M. S. Dresselhaus, and M. Tinkham, Phys. Rev. Lett. **93**, 167401 (2004).
[33] S. B. Cronin, A. K. Swan, M. S. Unlu, B. B. Goldberg, M. S. Dresselhaus, and M. Tinkham (unpublished).

Ab-Initio Simulations of the Growth and Structural Properties of Short Carbon Nanobells

G. L. Zhao[1,a], D. Bagayoko[1], and E. G. Wang[2]

[1]Department of Physics, Southern University and A & M College
Baton Rouge, Louisiana 70813, USA
[a] E-mail address: zhao@grant.phys.subr.edu
[2]State Key Laboratory for Surface Physics, Institute of Physics,
Chinese Academy of Sciences, Beijing, 100080, P. R. China

Keywords: carbon nanobells, carbon nanotubes, growth and structural properties of nanobells.

Abstract: We performed ab-initio density functional simulations to study the structural and growth properties of short carbon nanobells. We used a real space approach and the linear combination of atomic orbitals (LCAO) formalism. In the nitrogen-doped carbon nanobells, the nitrogen atoms that are attracted to the open-edge sites of the carbon nanobells play an important role in the growth of the short carbon nanostructures. We present the calculated electronic structure of the short nanobells. The calculated local density of states of the nanobells revealed field emission characteristics that agree with experimental observations.

I. Introduction

The carbon nanostructures present interesting properties with a great potential of applications. Particularly, short carbon nanotubes or carbon nanobells present excellent field-emission properties that have attracted a great interest for applications.[1-8] Experiments demonstrated that the nitrogen-assisted synthesis can grow carbon nanofibers on a large scale.[9-12] Such carbon nanofibers exhibit a "bamboo-like" structure. Distinctively, a great part of the bamboo-like nanofibers consists of short carbon nanobells. Individual nanobells are self-contained and stack one on top of the other to create a long nanofiber. The carbon nanobells may be viewed as short nanotubes such that their lengths are of the same order as their diameters. The electronic structure of the short carbon nanobells is substantially different from that of the pure and long carbon nanotubes because of the quantum effects inherent to their sizes. The nanobells exhibit novel electron field emission properties with a turn-on field of electron emission as low as $0.8 V/\mu m$.[9,13] We performed ab-initio density functional calculations, aiming to understand the growth, structural, and electronic properties of short carbon nanobells.

II. Method

Although the experimental synthesis of carbon nanobells produced samples of various sizes, measurements revealed that the atomic structure of the bamboo-like morphology in thick nanobells is similar to that of the thinner ones.[9] Experiments also revealed that adjacent nanobells do not have a firm contact, but instead the closed end of one nanobell is weakly inserted into the open end of another. Single nanobells can be easily separated from other part of the nanofiber.[10] Hence, our ab-initio calculations will focus on single nanobells. The weak interaction between adjacent carbon nanobells may be included as a perturbation in further studies in modeling the bamboo-like morphology of the nanofibers. We constructed a prototypical

in the inner rings, away from the open-edge of the nanobell. This result indicates that the effect of further relaxation of the third atomic ring and inner rings would be insignificant.

(B). A Possible Growth Mechanism of Carbon Nanobells. The growth mechanism of the carbon nanobells remains a difficult problem. There are probably two major growth models.[1] The first one assumes that the carbon atoms are added at the open-ends of the nanobells. [1,11] The second one involves the C_2 absorption process that is assisted by the pentagonal defects on the closed caps.[1] Although both models are very interesting, we have technical difficulties using density functional computations to simulate the second growth model. We successfully performed local density functional computations to test the first growth mechanism. Because of the active dangling bonds of carbon atoms at the open-edge of nanobells, there is a high possibility that carbon atoms can be attracted to these sites for growth to occur. We calculated the total energies in the following two cases. In the first case, a ring of 20 carbon atoms attaches to the open-edge of the carbon nanobell at a bond-length of 1.415 $\mathring{A}$. In the second case, these 20 carbon atoms are free. The calculated total energy in case I is substantially lower than the corresponding value in case II. The total energy difference, which may also be defined as the cohesive energy of the carbon atoms in the first growth model, is 4.7 eV/atom. In this growth model, see Fig. 1, C_2 dimers are absorbed at the active dangling bond sites at the open end of the carbon nanobell. A C_2 dimer that deposits on the open-edge of the bell forms one covalent bond on the same atomic ring. Each of the C atoms also forms one covalent bond with the C atom of the next atomic ring and remains an active dangling bond towards the open-space. This grow model is consistent with previous analysis of experimental results.[11,13, 21] Although we cannot rule out the second growth model (growth on the closed cap of carbon nanobells), our calculations presented a clear evidence that the first growth mechanism is highly possible.

(C). Nitrogen-Doped Carbon Nanobell. Experimental results indicated that the growth of the short carbon nanobells is highly dependent on the nitrogen concentration in the gas mixture during the synthesis.[9,10] Without nitrogen atoms in the growth gas mixture under the same conditions, long and pure carbon nanotubes, without the "bamboo-like" morphology, are produced. However, it was not clear why the nitrogen atoms could turn the growth of the would-be long carbon nanotubes into that of short carbon nanobells. We performed total energy calculations to study the nitrogen-doped carbon nanobells (CN_x nanobells). Since nitrogen atoms can also form the planar sp^2-hybrid,[22] we studied the substitutional doping of nitrogen atoms in the CN_x nanobells. The substitutional doping of nitrogen atoms in CN_x nanobells was also proposed from the analysis of experimental results.[13]

We first replaced carbon atoms with nitrogen atoms at the open-edge of the prototypical nanobell. We compared the total energies in the two cases. In the first case, computations are carried out for the pristine carbon nanobell in the presence of ten free atoms of nitrogen. In the second case, ten nitrogen atoms replace ten carbon atoms on the open-edge and the substitutionally N-doped nanobell is in the presence of ten free atoms of carbon. The calculated total energy in the second case is lower than that in the first case by an amount of 0.5 eV per atom, without relaxing the structure. We then performed total energy calculations and identified the atomic positions of the relaxed structure of the nitrogen-doped nanobell from the total energy minimization. The calculated C-N bond length in the first atomic ring at the

about 0.08 states per eV per atom. Thus, electrons will be emitted from the atomic sites near the open-edge of the nanobell in field-emission experiments. The LDOS of Fig. 2 exhibit a nearly metallic behavior. The real nanobell samples in experimental studies mostly involve multilayers of graphite sheets and the nanobells stacked one on top of the other. The weak interactions between graphite layers in these nanobells and that between the bells may further broaden the electronic energy levels. Consequently, a metallic behavior may be observable in the measurements of the electronic structure of N-doped nanobells.

IV. Conclusion

In conclusion, we performed ab-initio density functional calculations to simulate the growth, structural, and electronic properties of prototypical carbon nanobells. In the nitrogen-doped carbon nanobells, nitrogen atoms that are attracted to the open-edge of the nanobells may play a role of stopper of the growth of the nanostructures. The calculated local densities of states of the CN_x nanobells indicate that electrons are most likely emitted from the atomic sites near the open-edge of the carbon nanobell in field-emission experiments. This result agrees with experimental observations.

Acknowledgements: This work was funded in part by the US Department of the Navy, Office of Naval Research (ONR Award No: N00014-05-1-0009) and by US NASA (Award No. NCC 2-1344).

References

[1] M. S. Dresselhaus, G. Dresselhaus, and P. C. Eklund: Science of Fullerenes and Carbon Nanotubes, (Academic Press, New York, 1996).
[2] Walt A. de Heer, A. Châtelain, D. Ugarte: Science, Vol. **270** (1995), 1179.
[3] A. G. Rinzler, et al: Science, Vol. **269** (1995), 1550.
[4] Q. H. Wang, et al: Appl. Phys. Lett. Vol. **70** (1997), 3308
[5] Q. H. Wang, et al: Appl. Phys. Lett. Vol. **72** (1998), 2912.
[6] Y. Chen, et al: Appl. Phys. Lett. Vol. **73** (1998), 2119.
[7] K. A. Dean and B. R. Chalamala: Appl. Phys. Lett. Vol. **76** (2000), 375.
[8] J. M. Bonard, et al: Phys. Rev. Lett. Vol. **81** (1998), 1441.
[9] X. Ma, E. Wang, W. Zhou, D. A. Jefferson, J. Chen, S. Deng, N. Xu, and J. Yuan: Appl. Phys. Lett. Vol. **75** (1999), 3105.
[10] X. Ma, E. G. Wang, R. D. Tilley, D. A. Jefferson, and W. Zhou: Appl. Phys. Lett. Vol. **77** (2000), 4136.
[11] X. Ma, and E. G. Wang: Appl. Phys. Lett. Vol. **78** (2001), 978.
[12] E. G. Wang, et al: Carbon Vol. 41 (2003), p.1827.
[13] D. Y. Zhong , S. Liu, G. Y. Zhang, E. G. Wang: J. of Appl. Phys. Vol. **89** (2001), 5939.
[14] P. Hohenberg and W. Kohn: *Phys. Rev.* Vol. **136** (1964), B864; W. Kohn and L. J. Sham: *Phys. Rev.* Vol. **140** (1965), A1133.
[15] G. L. Zhao, D. Bagayoko, and L. Yang: Phys. Rev. B vol. Vol. **69** (2004), 245416.
[16] J. Callaway and N. H. March: *Solid State Physics*, vol. 38, Edited by H. Ehrenreich, D. Turnbull, and D. Seitz, (Academic Press, New York, 1984), p.135.
[17] G. L. Zhao, D. Bagayoko, and E. G. Wang: Modern Physics Letters B, vol. 17 (2003), 375.
[18] D. Bagayoko, G. L. Zhao, J. D. Fan, and J. T. Wang: *Journal of Physics: Condensed Matter*, Vol. **10** , (1998), 5645.
[19] S. G. Mikhlin: *The Numerical Performance of Variational Methods*, (Wolters-Noordhoff Publishing, 1971), ch.1, 2, & 7.
[20] S. H. Gould: *Variational Methods for Eigenvalue Problems*, (University of Toronto Press, 1957), ch. 2.
[21] J. Gavillet, A. Loiseau, C. Journet, F. Willaime, F. Daucastelle, and J. C. Charlier: Phys. Rev. Lett. Vol. **87** (2001), article #275504.
[22] W. A. Harrison: Electronic Structure and the Properties of Solids, (W. H. Freeman and Company, San Francisco, 1980), p. 91.
[23] CRC Handbook of Chemistry and Physics, Edited by R. C. Weast. D. R. Lied, M. J. Astle, and W. H. Beyer, (CRC Press, Boca Raton, Florida, 1990), p. F-188.

A Universal Relation between the Densities of States near Van Hove Singularities and the Effective Electron Masses in 1-Dimensional Semiconductors

G. L. Zhao* and D. Bagayoko

Department of Physics, Southern University and A & M College
Baton Rouge, Louisiana 70813, USA
* E-mail address: zhao@grant.phys.subr.edu

Keywords: nanotubes, 1-D semiconductors, electron masses, van Hove singularities.

Abstract. We present a universal relation between the densities of states near Van Hove singularities and the effective electron masses in 1-dimensional (1-D) semiconductors. The relation can be utilized as a new method to determine the effective masses of charge carriers of 1-D semiconductors in theoretical calculations and in experimental measurements. The calculated results, utilizing the relation for 1-D single-walled carbon nanotubes (SWCNTs), agree well with that of the conventional calculations when both approaches utilize the outputs of ab-initio density functional computations.

I. Introduction.

One-dimensional (1-D) materials, such as carbon nanotubes (CNTs), have emerged as attractive materials for applications in molecular-scale electronics.[i,ii] The electronic properties of 1-D CNTs have been extensively studied in recent years using various experimental tools and theoretical calculations.[ii,iii,iv] Particularly, scanning tunneling microscopy (STM) is a favorable tool for measuring atomic structures, density of states (DOS) of electrons, Van Hove singularities, and energy band gaps. However, there are some other physical quantities that require further studies. One of them is the effective mass of charge carriers (electrons or holes), an important physical quantity that characterizes the electronic transport properties of materials. Here, we present a universal relation between the densities of states of electrons near Van Hove singularities and effective electron masses in 1-D materials. This relation can be used as a new method to determine the effective masses of charge carriers in any 1-D semiconductors.

II. Densities of States and Effective Masses in 1-D Materials.

The electron density of states (DOS) per unit cell, G(ε), of a 1-D material can be calculated by the following expression.[v]

$$G(\varepsilon) = \frac{L}{2\pi} \sum_{(\varepsilon_{ik}=\varepsilon)} \frac{1}{\left| \frac{d\varepsilon_{ik}}{dk} \right|} \qquad (1)$$

where ε_{ik} is the energy of the i-th electron band at point k in the irreducible Brillouin zone; and L is the length of the unit-cell.

At an extremal point of an electron energy band, the first derivative of the band energy with respect to the wave vector k is zero, that is $d\varepsilon_{ik}/dk = 0$. A Van Hove singularity occurs at this point.. We can then approximate the band dispersion as a parabolic

which the band dispersion follows Eq. (5). The density of states and the effective mass of this single band has been discussed in the previous section. We then identify the relation as,

$$\frac{\overline{m}_2^*}{m_1} = \left[\frac{D_2(\varepsilon+\varepsilon_1)}{2D_1(\varepsilon+\varepsilon_0)}\right]^2 \qquad (9)$$

where $\overline{m}_2^*$ and $D_2(\varepsilon)$ are the average effective mass and the density of states of the doubly degenerate bands, respectively.

$$\overline{m}_2^* = \frac{1}{4}\left[\sqrt{m_2^{(1)}} + \sqrt{m_2^{(2)}}\right]^2 \qquad (10)$$

where $m_2^{(1)} = \dfrac{\hbar^2}{2b_1}$ and $m_2^{(2)} = \dfrac{\hbar^2}{2b_2}$.

The above discussions can also be extended to three or more energy bands that are degenerate at an extremal point, but are not degenerate elsewhere.

IV. Applications.

Although there is a wealth of experimental results regarding the density of states of electrons in single-walled carbon nanotubes (SWCNTs),[ii,iii] the study of the effective masses of the charge carriers in these materials is far from complete. As a test case of the new method to study the effective masses of the charge carriers in 1-D materials, we applied Eq.(7) or (9) to some SWCNTs. We list some of the results in Table 1, where m_0 is the free electron mass. $E_v^{(1)}$ in Table 1 refers to the first valence band near the Fermi level (E_F), whereas $E_c^{(1)}$ refers to the first conduction bands from E_F. Em is the energy (in eV) of the top of a valence band or the bottom of a conduction band near its Van Hove singularity. The energy of the top of the first valence band ($E_v^{(1)}$) has been chosen to be zero in Table 1. "Deg" refers to the degeneracy of the bands. Dm (in states/eV) is the peak value of the density of states at the Van Hove singularity; it was used to calculate the effective mass $\overline{m}^*$ using the universal relation, Eq.(7) or (9). We utilized the effective mass of charge carriers of SWCNT (10, 0) at $E_v^{(1)}$ as the single reference for the calculations of the effective masses ($\overline{m}^*$) of other SWCNTs. As a comparison, we also calculated the effective mass m* using the results of the conventional method for which we utilized the ab-initio electronic structure calculations. We performed self-consistent, ab-initio density functional calculations to obtain the electronic structure of the SWCNTs, using a linear combination of atomic orbital (LCAO) method.[6-10] Particularly, the ab-initio calculations for the electronic structure of nonsymmorphic SWCNTs (8, 4) and (10, 5) are very difficult tasks, since there are 112 and 140 atoms in their tubule unit cells, respectively. The calculated results of the effective masses $\overline{m}^*$ of the charge carriers in SWCNTs utilizing the universal relation Eq. (7) or (9) agree very well with those from the conventional method of ab-initio electronic structure calculations, as demonstrated in Table 1.

Acknowledgments: the work was funded in part by the US Department of the Navy, Office of Naval Research (ONR Award No: N00014-05-1-0009) and by US NASA (Award No. NCC 2-1344).

Accepted for publication in the Proceedings of the 2005 National Conference of the National Society of Black Physicists (NSBP).

Local Density Functional Description of Electronic Properties of Wurtzite Zinc Oxide (w-ZnO)

D. Bagayoko, G. L. Zhao, and L. Franklin
Department of Physics
Southern University and A&M College
Baton Rouge, Louisiana 70813, USA

Contact information for the corresponding author: Diola Bagayoko, P. O. Box 11776, Southern University and A&M College, Baton Rouge, Louisiana 70813, USA; Telephone: 001-225-771-2730; Fax: 001-225-771-4341; E-mail: Bagayoko@aol.com

Abstract

We report calculated, electronic properties of wurtzite zinc oxide (w-ZnO). Unlike many previous theoretical works, our linear combination of atomic orbital (LCAO) calculations, implemented following the Bagayoko, Zhao, and Williams (BZW) method, employed a local density approximation (LDA) potential to obtain band gaps and other results in agreement with experiments. We discuss the band structures, the calculated direct band gap (3.2 to 3.3 eV), and the electron effective mass (0.25 to 0.26 m_0).

PACS Numbers 71.20.Nr, 71.15.Ap, 71.15.Mb

I. Introduction and Motivations

Nowotny et al [1] and Thomas [2] provided some of the earliest experimental data on wurtzite zinc oxide (w-ZnO), the former on the lattice parameters and the latter on the band gap. A representative set of measurements of the band gap of bulk w-ZnO shows a robust agreement on its low temperature value of 3.44 ± 0.06 eV. [1-7] This range, i.e., ± 0.06 eV, is much larger than experimental uncertainties; it simply reflects differences that a traceable to those of actual lattice constants, measurement techniques and temperatures, and other factors. Some of these factors (impurities, defects) are associated with the growth conditions of the samples. Srikant and Clarke [8] appear to have settled the debate on the room temperature band gap of w-ZnO. They utilized different measurement techniques to arrive at a value of 3.30 eV. These techniques included reflection and transmission absorption, ellipsometric spectroscopy, Fourier transform infrared (FTIR) spectroscopy, and photoluminescence. This multitude of measurement techniques avoided limitations reported to afflict some previous investigations that reported a room temperature band gap of bulk w-ZnO 0.1 and 0.2 eV below the currently accepted value of 3.30 eV. Other groups reported photoemission [9-11] results for the band structure, the electrons effective mass [12] and the bulk modulus [13].

Several groups [14-20] have reported measured band gaps for films of w-ZnO grown by a variety of techniques. These growth methods included spray pyrolisis [14], pulsed laser deposition [16,18], cathodic electrodeposition in aqueous solutions [17], ion layer gas reaction (ILGAR) and rf magnetron sputtering [19], and plasma enhanced chemical vapor

LDA) effective masses of 0.25 (0.21), 0.25 (0.21), and 0.21 (0.18) m_0 in the k_x, k_y, and k_z directions respectively, where the values between parentheses resulted from their LDA calculations. These results were obtained for experimental lattice constants of 3.24961 Å , 5.20653 Å and u parameter of 0.345. Lambrecht et al. [33] noted that their calculated values of 0.23 m_0 and 0.21 m_0, in the parallel and perpendicular directions, are likely to be underestimates. Xu and Ching [35] reported 0.37, 0.28, and 0.32 m_0 in the Γ-K, Γ-A, and Γ-M directions in the Brillouin zone, for lattice constants given in Table 1. These authors utilized the orthogonalized LCAO formalism and employed a local density potential plus additional exchange derived with Wigner's interpolation. The 1966 measurements by Baer [12] found the electron effective mass for w-ZnO to be 0.24 $\pm$ 0.02 m_0. The above LDA results for the electron effective mass are uniformly lower than this experimental value.

The above overview of previous theoretical results, with the general disagreement between calculations, on the one hand, and between calculations and the firmly established experimental data, on the other hand, provides the motivation for this work. The wide spread of the LDA results for the band gap of w-ZnO, from 0.23 to 2.26 eV, suggests that limitations other than those genuinely attributable to the potential affected these results. Since 1998, Bagayoko, Zhao, and Williams have introduced a computational method [36-39] that clearly showed that *LDA potentials are no longer known to lead to woeful underestimates of the band gap of semiconductors.* Indeed, using the Rayleigh theorem, these authors introduced a new form of convergence for variational computations that utilize a basis set. The need to seek methodically [36-37] a basis set whose size is converged [i.e., the optimal basis set] vis a vis the description of the *occupied* states, they argued, straightforwardly arises from (a) the use of *only* the wave functions of the *occupied states* to construct the charge density, the potential, and the Hamiltonian in the iterative process and (b) the Rayleigh theorem that asserts the possible, continuing lowering of some unoccupied energies or bands when basis sets larger than the optimal one are utilized. This extra-lowering of some unoccupied energies, even though the physics (i.e., the Hamiltonian) is no longer changing, was identified as a basis set and variational effect that has afflicted most of the previous calculations, including those utilizing the generalized gradient approximation (GGA) of density functional theory (DFT) [40-41] and the GWA approximation [42]. Hence, the clear motivation of this work is to utilize properly, as per the BZW method, a local density potential to describe the electronic and related properties of w-ZnO. In the remaining of this article, we briefly present our method and discuss our results, which are basically in agreement with experiment, particularly as compared to previous, theoretical ones.

II. Method

Our computational method has been extensively described in previous publications [36-39]. It is characterized by the use of a local density approximation (LDA) potential [43] as parameterized by Vosko et al [44], the well-known linear combination of Gaussian orbitals (LCGO), and the rigorous application of the BZW method in carrying out the calculations. We utilized a program package developed and refined over decades [45-46].

III. Results

Some of our calculated band structures are shown in Figures 1 and 2. Figure 1 illustrates the dramatic differences between our results and those or previous LDA and other calculations. Essentially, there are no major differences between our calculated occupied bands and some previously reported ones. For the unoccupied bands, however, our results are distinctively far those of previous calculations. In Figure 1, the lowest unoccupied energy at the Γ point is shifted downward by approximately 2.2 eV as compared to its value obtained with the optimal basis set. Clearly, the differences between the low energy conduction bands from calculation II and III are far from those expected from a rigid shift. Hence, they cannot be corrected with simplistic "scissors" operations.

The above differences between our calculated conduction bands and those in previous reports explain the reason our calculated band gaps of 3.2 and 3.278 eV, at lattice constants specified in Table 1 and Figures 1 and 2, are very close to experimentally measured values. The differences between our results from the calculation at the experimental lattice constants in Figure 2 and the one just below it, in Table 1, are mainly due to the difference in the value of u, given that the lattice parameters are not far apart. Schröer and coworkers found a similar situation in their LMTO and GWA calculations. [27] The value of u, understandably, strongly influences that of the band gap.

Our calculated, total (DOS) and partial density of states (pDOS) in Figures 3 and 4 naturally reflect the differences discussed above for the electronic energy bands. In particular, the location of the lowest conduction bands with respect to the Fermi energy in these figures is drastically different from that in most of the previous theoretical investigations. The inset in Figure 3 illustrates our concept of a practical band gap. [37] Essentially, due to instrumental sensitivity, analysis techniques, and related uncertainties, an experimental work could find values of the band gap from the theoretical minimum of 3.278 to close to 4.0 eV. This possibility, practically non-existent in highly sensitive photoluminescence measurements, increases to a likelihood if simple optical absorption is the sole measurement technique. The determination of the onset of the band edge absorption is a source of large uncertainties, in addition to the fitting often involved in the determination of the band gap.

The electron effective masses from our calculations exhibit a slight anisotropy, as expected in a wurtzite structure. The effective mass is a measure of the curvature of the calculated bands. The agreement between calculated and measured effective masses indicates an accurate determination of the shape of the bands. We calculated the effective masses of the n-type carriers of ZnO, using the electronic structure from calculation II (the solid line in Fig. 1). Near the bottom of the lowest conduction band at the gamma point, we obtained 0.254, 0.260, and 0.264 m_0 in the Γ-A, Γ–K, and Γ-M directions, respectively, for the lattice constants in Figure 1. For the conduction band in Figure 2, the corresponding values are 0.257, 0.258, and 0.257 m_0 respectively. These values agree very well with the measured value of 0.24 m_0, within the experimental uncertainty [12] of 0.02 m_0, and with the experimental value of 0.275 m_o. [48] The above excellent agreement with experiment and the underestimates from previous LDA

[13] S. Desgreniers, Phys. Rev. B 58, 14102 (1998).
[14] S. A. Studenikin, N. Golego, and M. Cocivera, J. Appl. Phys. 83, 2104 (1998).
[15] P. L. Washington, H. C. Ong, J. Y. Dai, and R. P. H. Chang, Appl. Phys. Lett. 72, 3261 (1998).
[16] J. F. Muth, R. M Kolbas, A. K. Sharma, S. Oktyabrsky, and J. Narayan, J. Appl. Phys. 85,7884 (1999).
[17] Th. Pauporté and D. Lincot, Appl. Phys. Lett. 75, 3817 (1999).
[18] X. W. Sun and H. S. Kwok, J. Appl. Phys. 86, 408 (1999).
[19] M. Rebien, W. Henrion, M. Bär, and Ch. -H. Fischer, Appl. Phys. Lett. 80, 3518 (2002).
[20] B. S. Li, Y. C. Liu, Z. Z. Zhi, D. Z. Shen, Y. M. Lu, J. Y. Zhang, X. G. Kong, X. W. Fan, Thin Solid Films 414, 170-174 (2002).
[21] J. E. Jaffe, R. Pandey and A. B. Kunz, J. Phys. Chem. Solids 52, 755 (1991).
[22] J. E. Jaffe and A. C. Hess, Phys. Rev. B 48, 7903 (1993).
[23] S. Massidda, R. Resta, M. Posternak, and A. Baldereschi, Phys. Rev. B 52, 16977 (1995).
[24] H. Karzel, W. Potzel, M. Köfferlein, W. Schiessl, M. Steiner, U. Hiller, G. M. Kalvius, D. W. Mitchell, T. P. Das, P. Blaha, K. Schwarz, and M. P. Pasternak, Phys. Rev. B 53, 11425 (1996).
[25] J. R. Chelikowsky, Solid State Comm. 22, 351 (1977).
[26] U. Rössler, Phys. Rev. 184, 733 (1969).
[27] P. Schröer, P. Krüger, and J. Pollmann, Phys. Rev. B 47 6971 (1993).
[28] D. Vogel, P. Krüger, and J. Pollmann, Phys. Rev. B 52, 14316 (1995).
[29] Salehpour and S. Satpathy, unpublished, as cited by others.
[30] M. Usuda, N. Hamada, T. Kotani, and M. van Schilfgaarde, Phys. Rev. B 66, 125101 (2002).
[31] M. Oshikiri and F. Aryasetiawan, Journal of Physical Society of Japan 69, 2113 (2000).
[32] A. Svane and E. Antoncik, Phys. Rev. B, 33, 7462 (1986).
[33] W. R. L. Lambrecht, A. V. Rodina, S. Limpijumnong, B. Segall, and B. K. Meyer Phys. Rev. B 65, 075207 (2002).
[34] M. Oshikiri, F. Aryasetiawan, Y. Imanaka, and G. Kido, Phys. Rev. B 66, 125204 (2002).
[35] Y. -N. Xu and W. Y. Ching, Phys. Rev. B 48, 4335 (1993).
[36] D. Bagayoko, G. L. Zhao, J. D. Fan, and J. T. Wang, Journal of Physics: Condensed Matter, 10, 5645 (1998).
[37] G. L. Zhao, D. Bagayoko, and T. D. Williams, Physical Review B 60, 1563 (1999).
[38] G. L. Zhao and D. Bagayoko, New Journal of Physics, 2, 16.1-16.12 (2000), online 18 July 2000.
[39] G. L. Zhao, D. Bagayoko, and E. G. Wang, Accepted for publication in Phys. Rev. B 69, 1 (2004).
[40] P. Hohenberg and W. Koim, Phys. Rev. 136, B864 (1964).
[41] W. Kohn and L. J. Sham, Phys. Rev. 140, A1133 (1965).
[42] L. Hedin and S. Lundqvist, Solid State Physics 23, 1 (1969).
[43] D. M. Ceperley and B. J. Alder, Phys. Rev. Lett. 45, 566 (1980).
[44] S. H. Vosko, L. Wilk, and M. Nusair, Can. J. Phys. 58, 1200 (1980).

Table 1. Calculated, fundamental band gaps (Eg, in eV) of w-ZnO, along with pertinent lattice constants in Angstroms, compared to experiment. Numbers in the last four columns, for a given row, are from the reference cited in that row.

	Computational Method	**a (Å)**	**c (Å)**	**u**	**Eg (eV)**
Local Density Approximation (LDA) Potentials	LCAO-BZW (Present work)	3.2501	5.2071	0.3817	3.20
		3.2496	**5.206**	**0.345**	**3.28**
		3.2530	5.2130	0.3817	3.21
		3.2700	5.1800	0.381	3.22
	Zn^{2+} Pseudopotential	3.25	5.21		2.13[a]
	Zn^{12+} Pseudopotential	3.25	5.21		0.23[a]
	Pseudopotential	3.23	5.18		0.23[b]
	APW				1.40[c]
	LAPW	3.253	5.2129	0.3817	0.77[d]
	FLAPW				0.93[e]
	LMTO	3.2427	5.1948	0.3826	1.15[f]
	LMTO	3.2496	5.2065	0.345	0.97[f]
	LMTO	3.253	5.2129	0.3825	0.78[d]
	LMTO (cubic, a=4.57 Å)				2.26[g]
	FP-LMTO			0.382	1.813[h]
LDA & Additional Exchange	Orthogonalized LCAO	3.249	5.207	0.345	0.88[i]
LDA+SIC	Pseudopotential	3.29	5.29		3.77[b]
X^{α} Potential	Pseudopotential	3.25	5.21		1.58[a]
GWA	LMTO	3.2427	5.1948	0.3826	4.28 and 4.06[a]
GWA	LMTO	3.2496	5.2065	0.345	3.45 and 3.63[a]
GWA	LMTO	3.253	5.2129	0.3825	2.44[d]
GWA	LAPW	3.253	5.2129	0.3817	2.44[d]
Model GWA	FLAPW				4.23[e]
Empirical Pseudopotential (EMP)					3.5[j]
Empirical KKR					3.30[k]
Experiment (Bulk, Low Temperatures)					**3.44**
Experiment (Bulk, Room Temperature)					**3.30**

[a]Reference 27 [b]Reference 28 [c]Reference 29
[d]Reference 30 [e]Reference 23 [f]Reference 31
[g]Reference 32 [h]Reference 33 [i]Reference 35
[j]Reference 25 [k]Reference 26

Figure 2. Calculated band structure of wurtzite zinc oxide (w-ZnO), as obtained with BZW method, for experimental lattice constants of $a = 3.2496$ Å, $c = 5.206$ Å, and $u = 0.345$. The band gap is 3.278 eV.

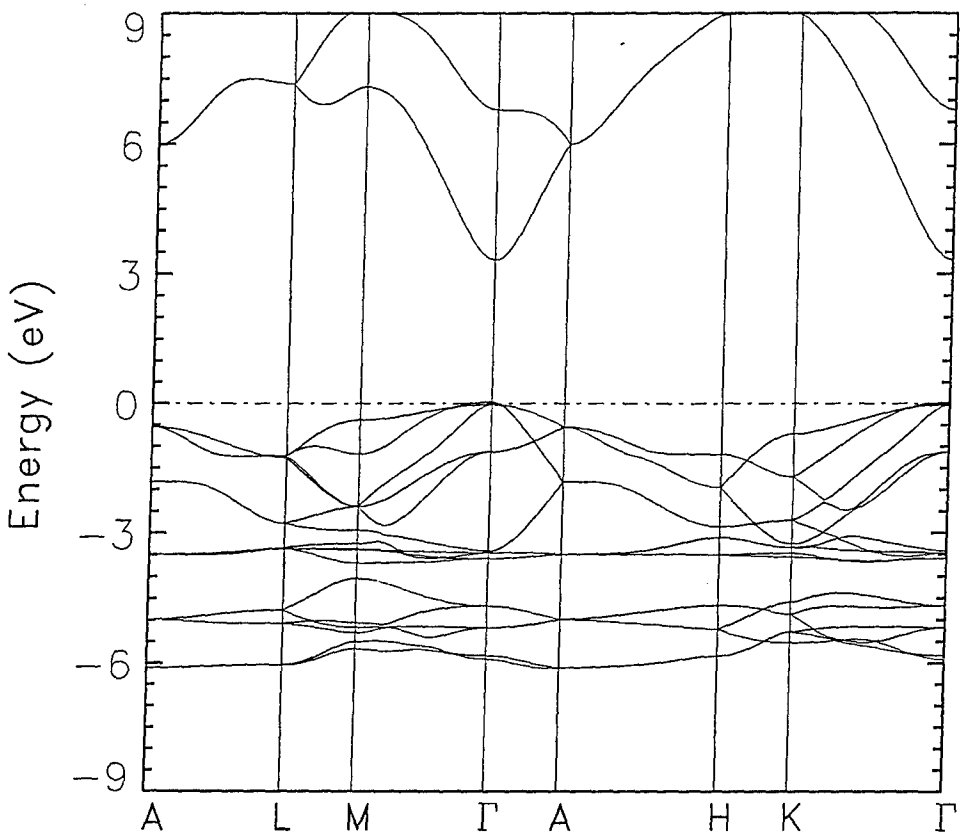

Figure 4. Calculated partial density of states (pDOS) for w-ZnO at the experimental lattice constants of $a = 3.2496$ Å, $c = 5.206$ Å, and $u = 0.345$. The graph illustrates the influence of the zinc d and the oxygen p in the upper valence bands. Zinc s dominates in the lowest conduction band.

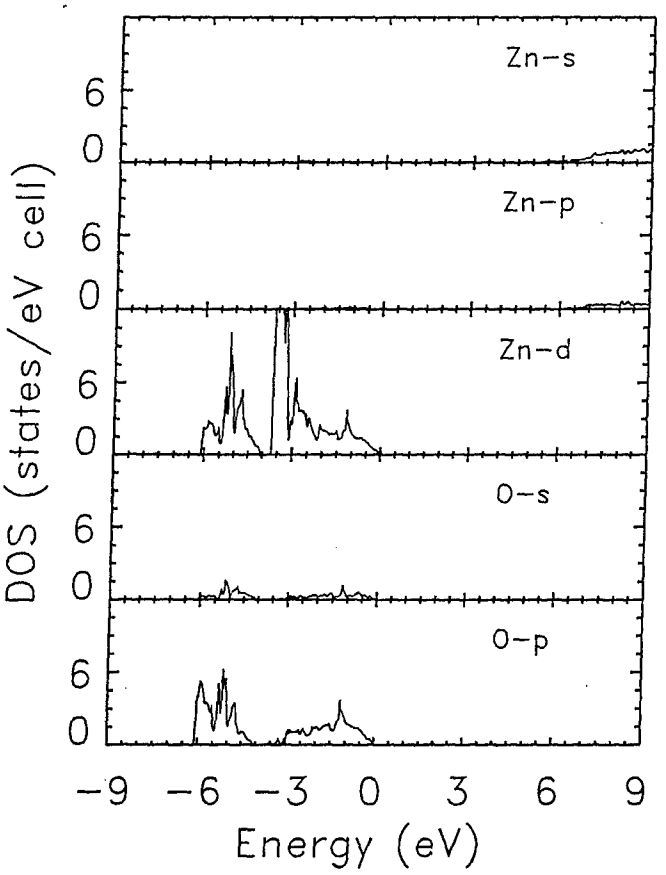

Reprinted from

JOURNAL OF APPLIED PHYSICS

Vol. 96, No. 8, 15 October 2004

Predictions of electronic, structural, and elastic properties of cubic InN

D. Bagayoko, L. Franklin, and G. L. Zhao
Department of Physics, Southern University and A&M College, Baton Rouge, Louisiana 70813

pp. 4297-4301

AMERICAN INSTITUTE OF PHYSICS

TABLE I. Experimental and theoretical lattice constants (a, in angstroms) for *c*-InN, along with the calculated values of the bulk modulus gigapascal and of the fundamental band gap (eV). Results in the last three columns, for a given row, are from the reference cited in that row.

	Computational Method	a(Å)	B(GPa)	Eg(eV)
Local Density Approximation (LDA) Potentials	LCAO-BZW (Present work)	5.017	145	+0.65
		4.98		+0.74
	Pseudopotential Method (PP)	4.95	145	−0.36[a]
		5.004	140	−0.40[b]
		4.95	145[c]	
		4.97[d]		
		4.932	140	−0.35[e]
		4.788	155[f]	
				−0.18[g]
	LAPW	4.94	145[c]	
	Full potential LAPW	5.03	138	−0.11[h]
				−0.48[h]
	Full Potential LMTO	4.92	139[j]	−0.4[i]
	Atomic sphere approximation (ASA)			−0.1[l]
				+0.02 and +0.08[k]
Generalized gradient approximation (GGA)	PP	5.06	120[c]	
		5.109	118	−0.55[b]
LDA plus self-interaction correction (SIC)		5.05[d]		+0.43[a]
QP Calculation	PP			+0.52[a]
QP+SIC	PP			+1.31[a]
DFT Exact Exchange				+1.4[g]
DFT, SX	ASA			+1.3[i]
Estimate of the bulk modulus of zinc-blende indium nitride (*c*-InN) using elastic properties of wurtzite InN			137[l]	
Empirical Pseudopotential Calculations (EMP)				+0.592[m]
Experimental: Measured lattice constants		4.97±0.01[n]		
		4.98[o]		
		4.986[p]		

[a]Reference 10.
[b]Reference 13.
[c]Reference 11.
[d]Reference 15.
[e]Reference 18.
[f]Reference 21.
[g]Reference 14.
[h]Reference 12.
[i]Reference 16.
[j]Reference 17.
[k]Reference 19.
[l]Reference 20.
[m]Reference 22.
[n]Reference 7.
[o]Reference 8.
[p]Reference 9.

II. METHOD AND COMPUTATIONAL DETAILS

We performed zero temperature, nonrelativistic calculations of the electronic and related properties of *c*-InN. Our *ab inito*, self-consistent calculations employed the local density approximation potential of Ceperley and Alder[27] as parametrized by Perdew and Zunger.[28] As stated above, we used the LCAO. The feature distinguishing our computational method from the previous investigations noted above consists of our implementation of the BZW procedure. In so doing, we started the calculations for *c*-InN with a minimal basis set. We subsequently performed several other self-consistent calculations with larger and larger basis sets. The basis set for any of these calculations was obtained by augmenting the one for the previous calculation with the orbital describing the next excited level of the atomic or ionic species present in the system. The occupied bands of a given calculation are compared to those of the previous. These comparisons, particularly for the first two calculations, often show differences (in numerical values, branching, or curvature). This process continues until the occupied energies from a calculation are equal, within computational uncertainties, to their corresponding ones from the calculation that follows it. Then, the output of the former calculation provides the physical description of the material under study and the related basis set is dubbed the optimal basis set. According to the Rayleigh theorem,[26] some of the *unoccupied bands* from the latter may be lower than their counterpart from the former.[24–26,29,30]

The above additional lowering is the *basis set* and *variational* effect inherently associated with variational calculations of the Rayleigh-Ritz type. In the iterative process, the use of the wave functions for the occupied states *only* in the construction of the charge density, and hence the potential and the Hamiltonian, ensures the exhaustion of the accounting for the physical interactions when the occupied energies converge vis-a-vis the size of the basis set. As fully explained elsewhere,[24–26,29] however, some unoccupied energies will continue to be lowered as the basis set is increased beyond the optimal one. The sizes of the minimal and optimal basis sets vary vastly with the type of functions in the

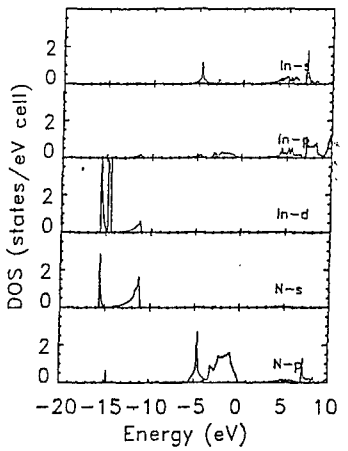

FIG. 3. pDOS for zinc-blende indium nitride (c-InN) as obtained with the bands shown in Fig. 1. The dominance of nitrogen p at the top of the valence band is obvious in this graph.

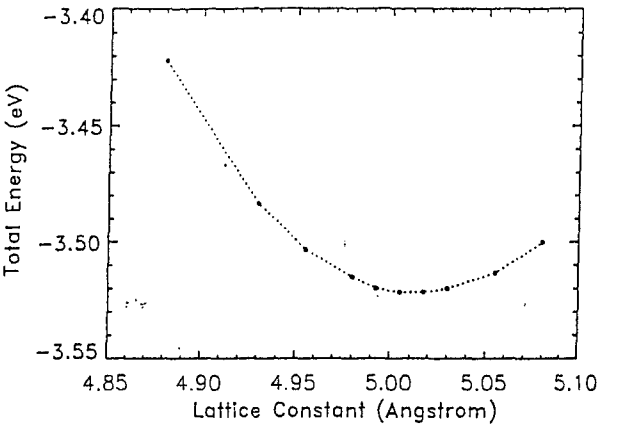

FIG. 4. Total energy of (c-InN) vs the lattice constant. The total energy at the equilibrium lattice constant of 5.017 Å is 1949.4215 eV.

the latest experimental one of 4.986 Å. Our calculated bulk modulus of 145 GPa is close to the results from some other LDA calculations[10,11] and disagrees with findings around 120 GPa from GGA calculation[11,13] as shown in Table I. The tables for the calculated energies are expected to provide useful comparisons for future experimental investigations. Our calculated LDA-BZW band structure is drastically different from the findings of most of the previous calculations—as far as the unoccupied bands are concerned. The large differences between our calculated band gaps and previous LDA results in Table I are a direct consequence of the differences between the respective *unoccupied* bands.

The empirical pseudopotential (EMP) result[22] of 0.592 eV is relatively close to our findings of 0.65 and 0.74 eV. We cannot draw much fundamental significance from this fact, however, given that this EMP result was obtained using model potential parameters whose derivation entailed fitting to data that included a band gap of 0.59 eV. For the purposes of application, however, this closeness portends much importance. Indeed, we expect potential parameters derived from fitting to our data to lend themselves to credible and practical descriptions of electronic, optical, elastic, and structural properties of materials. This assertion is partly supported by the versatility and relative ease of empirical pseudopotential calculations.

As in the case of w-InN,[23] our results do not show any indication of an overestimation of the p-d repulsion by LDA potentials. This overestimation was believed[10] to be the source of the very small or negative band gaps by pushing the top of the valence band, dominated by p states, to higher energies. According to our findings, it is rather the extra lowering of the bottom of the conduction band that produces LDA band gaps that are negative or very small[23,25] if LCAO type computations do not utilize the BZW approach to avoid it while ensuring the adequacy (or convergence) of the basis set for the description of occupied states. In fact, the basic derivation of the ground state theory that is the original density functional theory[34,35] implicitly suggests such an approach, notwithstanding the need to account for the redistribution of electrons in molecular to solid environments with judicious polarization and diffuse orbitals.[36]

As per their definition, effective masses provide a measure of the quality (i.e., curvature) of band structures. Our LDA-BZW calculations found electron effective masses, at the bottom of the conduction band, of $0.065m_0$, $0.066m_0$, and $0.066m_0$ in the Γ-L, Γ-X, and Γ-K directions, respectively, for the equilibrium lattice constant. For a lattice constant of 4.98 Å, the corresponding effective masses for the electrons are $0.076m_0$, $0.073m_0$, and $0.073m_0$ in the Γ-L, Γ-X, and Γ-K directions, respectively. Our calculated, equilibrium, electron effective masses are very close to the $0.066m_0$ from the EMP calculations of Fritsch, Schmidt, and Grundmann.[22] This agreement supports our comment above relative to the potential use of EMP calculations when the potential parameters are derived in part by fitting to LDA-BZW results.

IV. CONCLUSION

In lieu of a conclusion, we contend that our *ab initio*, self-consistent LDA-BZW calculations have predicted electronic, structural, and elastic properties of cubic InN (c-InN) in the zinc-blende structure. It is hoped that experimental investigations will follow in the near future. It emerges from this work that theoretical efforts should be directed to the determination of actual limitations of LDA and of other approaches as opposed to echoing the chorus now known to be untenable, as per the physical interactions, and that ascribes to LDA a woeful underestimation of band gaps that is, as per the Rayleigh theorem, straightforwardly a consequence of a basis set and variational effect.

ACKNOWLEDGMENTS

This work was funded in part by the Department of the Navy, Office of Naval Research (ONR, Grant No. N00014-98-1-0748), NASA (Award Nos. NCC 2-1344 and NAG 5-10253), and by the National Science Foundation (Grant No. HRD 0000272). The authors are indebted to Dr. J. Wu for bringing the band gap problem for cubic InN to their attention.

[1]J. W. Orton and C. T. Foxon, Rep. Prog. Phys. 1 (1998).
[2]O. Ambacher, J. Phys. D 31, 2653 (1998).
[3]A. G. Bhuiyan, A. Hashimoto, and A. Yamamoto, J. Appl. Phys. 94, 2779 (2003).

Reprinted from

JOURNAL OF APPLIED PHYSICS

Vol. 97, No. 12, 15 June 2005

Density-functional theory band gap of wurtzite InN

D Bagayoko and Lashounda Franklin
Department of Physics, Southern University and A&M College, Baton Rouge, Louisiana 70813

pp 123708 1-5

AMERICAN INSTITUTE OF PHYSICS

gap of 1.5 eV. The linear combination of Gaussian orbital (LCGO) calculations of Xu and Ching[29] employed a LDA potential plus additional exchange effects obtained with Wigner interpolation formula. They reported a band gap of 1.02 eV. The LDA+C work of Wei *et al.*[27] augmented the LDA potential with atom-dependent corrections and obtained a band gap of 0.85 eV with an uncertainty of 0.1 eV.

Clearly, the above state of theoretical calculations is amply sufficient to motivate the present work. A recent experimental development[30] exacerbated the urgency of our theoretical investigations. Indeed, the concordant findings of the second group of experiments, described above, have just been questioned by Shubina *et al.*[30] in 2004. These authors showed the possibility of explaining the spectra of this second group of experiments not in terms of near-band-edge absorption or emission, but rather as manifestations of surface/gap states or Mie resonances due to In precipitates in InN. They noted the poor thermal stability of InN and the low In vapor pressure to support their position. Specifically, for high-quality InN films grown at $T>500$ °C by MBE or MOVPE, they utilized x-ray diffraction to observe tetragonal In precipitates in hexagonal InN. Their very low-temperature (0.35 K) measurements by thermally detected optical absorption (TDOA) indicate the possibility of having a band gap around 1.4 eV. The authors refrained from making a definitive statement as to the location of the fundamental band gap, despite their observations, due to the difficulties in separating the intraband absorption in InN from Mie resonances.

METHOD AND COMPUTATIONAL DETAILS

Our calculations employed the Ceperley and Alder[31] local-density-functional potential as parametrized by Perdew and Zunger[32] in an *ab initio* LCGO formalism. We also employed the GGA potential of Perdew and co-workers[33] which goes beyond LDA. The calculations are nonrelativistic and for zero temperature. A key distinction between this work and previous calculations resides in our utilization of the *ab initio* Bagayoko, Zhao, and Williams[34,35] (BZW) method in carrying out the self-consistent computations. Introduced[34] in 1998 and extensively employed[35–38] thereafter, this method rigorously avoids a basis set and variational effect inherently associated with all variational calculations that utilize both the linear combination of atomic orbital (LCAO) and a charge density obtained only with the wave functions of the occupied states. The effect, a consequence of the Rayleigh theorem, consists of a lowering of unoccupied energy levels or bands, which is not ascribable to a physical interaction, after the total convergence of the charge density, the potential, and of the occupied energy levels with respect to the size of the basis set.[34,35]

BZW self-consistent calculations begin with the minimum basis set, i.e., one that is just large enough to include all the orbitals for the occupied levels in the atomic species that are present in the system under study. This initial basis set, in our case, is derived from calculations for the atomic or ionic species present in the finite or infinite system under investigation. Completely self-consistent calculations with this basis set are generally not expected to describe the system correctly. Indeed, they generally do not account for electron redistribution in the system as opposed to that in neutral atoms or ionic species. A second self-consistent calculation is performed with a basis set that includes the minimum basis set as augmented with the orbital representing the lowest excited levels in the atomic (or ionic species). The occupied energy levels or bands of calculations I and II are compared. One generally finds differences between these energies from the two calculations. For solids, these differences are in numerical values and the branching and curvatures of the bands. A third calculation is performed by augmenting the basis set of calculation II as described above. If a comparison of the self-consistent, occupied energies of calculations II and III do not show a complete agreement, within applicable errors, the process of augmenting the basis set is continued. Eventually, calculations N and $(N+1)$ will have the same occupied energies. Further, the charge density and the potential, from these two calculations, are, respectively, the same.[34,35] Upon the convergence of the variational calculations with respect to the size of the basis, the results for calculation N are selected as the physical ones. One generally finds, indeed, that calculation $(N+1)$ produced some unoccupied energies that are lower than the corresponding ones in calculation N. These differences that vary vastly with the value of $\vec{k}$ in reciprocal space are manifestations of the aforementioned basis set and variational effect.[34–38] The basis set for calculation N is called the optimal basis set.

Other ordinary features of our calculations are thoroughly described in the literature in seminal papers that reported on the development[39–41] of the program package and its recent utilization.[34,35,38] We provide below computational details germane to a replication of our *ab initio* work. The experimental,[3] low-temperature wurtzite lattice parameters utilized in our work are $a=3.544$ Å, $c=5.718$ Å, and $u=0.3790$. Preliminary calculations for the neutral In and N atoms and the solid *w*-InN indicated that the self-consistent system is approximately $In^{0.8+}N^{0.8-}$. Consequently, we performed self-consistent calculations for In^{1+} and N^{1-} to obtain the input, "atomic" orbitals. The minimal basis set comprised atomic orbitals representing In^{1+} $(1s2s2p3s3p3d4s4p4d5s5p)$ and N^{1-} $(1s2s2p)$. We employed even-tempered Gaussian functions in the construction of the atomic orbitals. The s and p orbitals of In were described with 16 even-tempered Gaussian functions with the respective minimum and maximum exponents of 0.14 and 0.2300×10^6. The d orbitals for In entail 14 even-tempered Gaussian, the same as for the ones s and p at the exclusion of the two largest exponents. Similarly, the s and p orbitals of N were constructed using 13 even-tempered Gaussian exponents whose smallest and largest values were 0.124 215 and $0.136\,000\,5\times10^5$. The computations were generally completely self-consistent after 60 iterations. The convergence, for a given self-consistent calculation, was reached when the potential did not change by more than 10^{-5} from one iteration to the next. Upon reaching self-consistency, the error made in accounting for 72 electrons was 0.004 31.

TABLE I. Eigenvalues (eV), at some high symmetry points, for wurtzite indium nitride (w-InN) as obtained from LDA-BZW calculations for a=3.544 Å, c=5.718 Å, and u=0.3790. The Fermi energy of −0.222 12 eV is set to zero in the table.

A	L	M	H	K	Γ
−13.0972	−11.5668	−11.2329	−11.3021	−11.2827	−11.6988
−3.25532	−5.25538	−5.20231	−4.89999	−4.32501	−5.61294
−3.25532	−5.25538	−4.27059	−4.89999	−4.32501	−0.89662
−0.46069	−1.62671	−3.34893	−3.34349	−4.2695	−0.89662
−0.46069	−1.62671	−2.29475	−3.34349	−2.39761	−0.0049
−0.46069	−1.53365	−1.75651	−1.23894	−2.39761	0
−0.46069	−1.53365	−0.8656	−1.23894	−2.14019	0
3.366891	4.570732	4.748424	6.125875	6.740313	0.878663
3.367163	4.570732	6.175673	6.125875	6.740313	3.662409

the absorption, as per their Fig. 2(c) visibly commenced around 0.9 eV and reached a plateau at 2 eV, in accordance with our concept of practical band gap.

The LDA-BZW effective masses for the electron close to the bottom of the lowest conduction band at gamma show a slight anisotropy. The electron effective mass is around $0.088m_o$ in the plane perpendicular to k_z (from Γ to M and Γ to K) and $0.082m_o$, in the direction of k_z (from Γ to A), in the immediate vicinity of the gamma (Γ) point. The GGA-BZW calculations led to values of the electron effective mass very similar to the ones for LDA. Specifically, at the bottom of the lowest conduction band, they are 0.081, 0.077, and $0.082m_o$ from Γ to M, Γ to K, and Γ to A directions, respectively. These effective masses are also in agreement with experiment,[14] taking into account the quality and other features of the samples (i.e., temperature, pressure, electron concentrations). Wu *et al.*[14] obtained a value of 0.07 by using a band gap of 0.7 eV in their analysis. They also provided a plot of the electron effective mass as a function of electron concentration.

DISCUSSIONS

For a discussion of our results, we underscore the need for specificity relative to the lattice parameters, sample quality[30] and growth conditions,[11] temperature,[12] and electron concentration[11] when comparing results from different experimental investigations. In particular, the significant effect of electron concentration on the band gap[11,44–46] could explain the 0.75–0.8-eV band gap found by Wu *et al.*[12] whose samples had a relatively low electron concentration of 5×10^{18} cm^{-3}. Our calculated band gap of 0.88 eV agrees very well with the experimental result of 0.89 eV of Inishima *et al.*[11] for a sample with an electron concentration of 5×10^{19} cm^{-3}. As noted above in connection with the "practical band-gap," measurement techniques, the analysis of data, and related uncertainties are critical. Specifically, we reiterate that absorption techniques could lead to a value of the band gap of w-InN as large as 2 eV.

Some authors[22] evoked a p-d repulsion to explain the small (generally negative) band gap from previous LDA calculations. LDA is reported to overestimate this repulsion and to push upward the top of the valence band. Our results provide no indiction of such a limitation of LDA. Rather, they clearly show that the extra lowering of the bottom of the conduction band, on account of the Rayleigh theorem, straightforwardly leads to the band-gap problem in LDA and other variational calculations that employ a basis set. This work partly responds to the calls by Ghani *et al.*[44] and by Vurgaftman and Meyer[45] for revisiting the issue of the band gap of w-InN following their extensive compilations of experimental and theoretical results on indium nitride. Ghani *et al.* discussed the formation of oxynitrides (InON), particularly in aged or annealed polycrystalline samples, as a possible source for the increase of the band gap to values around 2 eV. These polycrystalline films are reported to be susceptible to containing a high density of oxygen atoms at their grain boundaries.

CONCLUSION

In conclusion, we claim to have resolved the controversy surrounding the band gap of wurtzite InN. We did so within the local-density approximation (LDA) with the BZW method. Unlike many schemes purporting to correct limitations of local-density approximation and that come with other approximations whose effects are at best ill understood, the *ab initio* BZW method is rigorously anchored on a mathematical theorem. The above points explain the reason this communication is hoped to end the echoing of the incorrect chorus claiming that it is well known that local-density approximation woefully underestimates the band gap of semiconductors and insulators. In the above sense, and even though this communication is devoted to wurtzite InN, the method applies to other calculations that employ basis sets in a variational scheme of the Rayleigh–Ritz type, as is the case in many energy level (finite systems) or band calculations. An utterly important point associated with the above points stems from the fact that the proliferation of schemes aimed at "correcting" limitations of LDA has started to look like that of epicycles in the Ptolemaic model of the solar system. A seriously unfortunate consequence of this situation consists of diverting efforts from grasping the actual capabilities and limitations of LDA and those of schemes aimed at going beyond the local-density approximation or beyond density-functional theory altogether.

Manuscript submitted to Phys. Rev. B

Reexamination of the Ab-Initio Calculation of the Electronic Structure of ZnSe, Ge, and GaAs

G. L. Zhao*, L. Franklin and D. Bagayoko
Department of Physics, Southern University and A & M College
Baton Rouge, Louisiana 70813 USA

Abstract

In this work, we reexamined some of the mathematical and physical properties of the ab-initio LCAO calculations for the electronic structure of ZnSe, Ge, and GaAs. The utilization of non-strongly minimal systems in the self-consistent ab-initio calculations could lead to a non-uniformity in approaching the solution in the Ritz-process. We performed test computations for the electronic structure of hydrogen atom. We have proposed that an optimum basis set may be needed so that the calculated electron density is converged and the significant scattering of the Ritz-coefficients may be avoided. We have applied the new method to the calculations of the electronic structure of ZnSe, Ge, and GaAs. Our calculated results of the electronic properties agree well with experimental data.

1 Introduction

Ab-initio density functional calculation is a very powerful tool to study the physical properties of materials, including semiconductors, metals, surfaces, interfaces, and others.[1, 2, 3, 4, 5, 6, 7] However, previous density functional calculations in local density approximation (LDA) for semiconductors or insulators often underestimated the band-gaps by 30-50 %.[8, 9, 10, 11] Closely related to the band-gap problem, the calculated effective masses of electrons (n-type carriers) and the optical properties of semiconductors –from previous LDA computations– also disagree with experimental results. There have been some theoretical efforts intended to address these problems, including the calculations that utilize nonlocal, energy-dependent, non-Hermitian self-energy operators.[12, 13, 14, 15, 16, 17, 18] Others implemented the exact exchange potentials or included the effects of core states via the exchange diagram.[19, 20, 21] Aryasetiawan and Gunnarsson reviewed several computational methods, including the GW method, aimed at describing excited state properties.[17]. Johnson and Ashcroft recently utilized simplified applications of the GW method to make scissors-type corrections to the band gaps of semiconductors.[18]

on the wave functions $\Psi_{\vec{k}i}$ of the occupied electron states, i. e.,

$$\rho(\vec{r}) = \sum_{\vec{k}i} f_{\vec{k}i} \mid \Psi_{\vec{k}i} \mid^2 \tag{2}$$

where $f_{\vec{k}i}$ is the Fermi distribution function. The solution of the Kohn-Sham equation has to satisfy a condition that

$$\int \rho(\vec{r}) dv = N \tag{3}$$

where N is the total number of electrons in the system. In this work, we implemented the formalism of the linear combination of atomic orbitals method to solve the Kohn-Sham equation. The essentials of the mathematical properties of the calculations are those of the Ritz-process of the variational calculations. We will follow the notations in the discussion of the variational theory according to S. G. Mikhlin[23].

In the LCAO method,[24, 25, 26, 27, 28, 29, 30, 31, 32] we solve the Kohn-Sham equation self-consistly. We expand the eigenfunction $\Psi_{\vec{k}i}$ of the effective single electron state of the many-atom system as a linear combination of the atomic wave functions, which is a Ritz process as termed in the variational theory according to Mikhlin's notations.[23]

$$\Psi_{\vec{k}i}(\vec{r}) = \sum_{\alpha m} C_{\alpha m}(\vec{k}i) \phi_{\alpha m}(\vec{k}, \vec{r}) \tag{4}$$

where $C_{\alpha m}$ are the expansion coefficient or the Ritz-coefficients; $\phi_{\alpha m}(\vec{k}, \vec{r})$ are Bloch wave functions which are expressed in terms of atomic wave functions as

$$\phi_{\alpha m}(\vec{k}, \vec{r}) = \frac{1}{\sqrt{N}} \sum_{l} e^{i\vec{k}.\vec{R}_l} u_{\alpha m}(\vec{r} - \vec{\tau}_m - \vec{R}_l) \tag{5}$$

where $u_{\alpha m}$ is the atomic wave function of the α-th state of the m-th atom at the position $\vec{\tau}_m$ and is the coordinate element in the energy space (or Hilbert space). The solution for the Ritz-coefficients $C_{\alpha m}$ of the Kohn-Sham equation is the one that the total energy functional $E_{total}(\rho)$ reaches its minimum.

2.2 The Requirement of Strongly Minimal Systems in the Ritz Process

We shall study the countable system of the coordinate elements in the Hilbert space, where

$$\{u_n\} = u_1, u_2, u_3, ..., u_n, ... \tag{6}$$

the onset of the computational instabilities in the LCAO method may not be marked by an occurrence of the negative eigen-value of the overlap matrix.

Mikhlin illustrated the problems of the utilization of non-strongly minimal systems in Ref. [23] by several examples. Generally, the non-strongly minimal systems will not reach a solution in the limit of $n \to \infty$ in the Ritz-process. For finite values of n, some of the non-strongly minimal systems may approximate the Ritz-coefficients with a tendency to stabilize non-uniformly for increasing n. Other non-strongly minimal systems may show that the Ritz-coefficients scatter significantly. The coefficients may change abruptly from one approximation to the next. One may not know the exact solution for the problem and has the difficulty of identifying an estimate for the error in the approximate solutions. There is so far no mathematical theorem that can identify exactly the properties of the instabilities in the utilization of non-strongly minimal systems in the Ritz-process. The relevant problems may include those such as the condition(s) that the instabilities may occur, the behavior of the instabilities, and the method(s) to identify them.

The problems became more complex in the applications of the numerical computations of the electronic structure of solid state materials, since most of the basis sets of various implementations of ab-initio density functional calculations are not strongly minimal. The true plane-wave basis set satisfies the condition to be strongly minimal. However, the requirement of the computational accuracy and the number of the true plane-waves in the solid state calculations are usually beyond the limitation of our computer resource at present. The orthogonalized plane waves, which are derived by the Schmitdt process to be orthogonal to the core wave functions, are not strongly minimal.

One may propose to orthogonalize the atomic orbitals for the solid state calculations. However, if the basis set is not strongly minimal, the orthogonalization of the basis set in solid state calculations may encounter the similar instability problem. The orthogonalization procedure of the basis set involves the computation of the inverse of the overlap matrix. If the smallest eigen-value of the overlap matrix approaches zero or negative, an instability problem may occur.

2.3 Consideration of Some Physical Properties

Although the true plane-wave basis set can be implemented in ab-initio density functional calculations of the electronic structure of solid state ma-

atomic wave functions, we performed ab-initio atomic calculations that also utilized density functional formalism. The radial parts of the atomic wave functions were expanded in terms of a linear combination of Gaussian orbitals (LCGO).

The electronic energy levels and related wave functions of hydrogen atom are exactly known from the analytical solution of the Schrödinger wave equation. We can test the numerical performance of the variational computations of the Ritz-process on hydrogen atom. We utilized the same ab-initio atomic computation program and the LCGO formalism to calculate the electronic structure of hydrogen atom. The Schrödinger wave equation for the calculation of the electronic structure of hydrogen atom is a one-electron problem, instead of the many-body problems such as those for the studies of solid state materials. In the ab-initio computation of the hydrogen atom using the LCGO method, we did not include the density functional potentials in the Hamiltonian. The Schrödinger wave equation for hydrogen atom is then a linear differential equation, instead of the non-linear differential equation such as the density functional Kohn-Sham equation. We compared the results of the numerical computations of hydrogen atom with the exact solution. In the numerical computations, we utilized basis sets of even-tempered Gaussian exponentials with a minimum of 0.10×10^{-2} and a maximum of 0.15×10^{4} in atomic unit. We used various sizes of the basis sets of the Gaussian functions.

In Fig. 1, we present the calculated electronic energy levels of hydrogen atom versus the total numbers of the utilized Gaussian functions (Gaussian orbitals). The solid, dotted, and dash-dotted lines in Fig. 1 present the calculated energy levels of s-, p-, and d-states of hydrogen atom, respectively. As the numbers of the Gaussian functions in the basis sets increase from 5 to 15, the calculated energy levels approach their converged values. The calculated first three energy levels of hydrogen atom converged to -1.0, -0.250, and -0.111 Ry, when we utilized $15 - 60$ Gaussian functions in the basis sets. These calculated energy levels of hydrogen atom agree very well with that of the exact solution for the principal quantum number $n = 1$, 2, and 3, respectively. The lowest energy level in Fig. 1 belongs to the 1s state of H atom. The second lowest level includes 2s and 2p states. The third one includes 3s, 3p, and 3d states.

When the numbers of the utilized Gaussian functions in the basis sets are larger than about 70, the calculated electron energy levels of the 3p and 3d states of hydrogen atom dropped to lower values than those of the exact solution. The features illustrate the instabilities of the variational calcu-

of the five self-consistent calculations. We first carried out completely self-consistent calculations for ZnSe using a basis set that included Zn(1s2s3s4s 2p3p 3d) and Se(1s2s3s4s 2p3p4p 3d) orbitals. We then repeated the self-consistent calculation using the above basis set as augmented by the orbitals describing the next lowest-lying energy level of Zinc. Hence, Zn(4p) orbitals were added to basis set I. We then plotted the energy bands from these two distinct calculations, i.e., calculation I and II, and compared them numerically and graphically. Differences were obvious. We then performed calculation III and compared its results to those of calculation II. Up to five self-consistent calculations were performed and the results of each calculation were compared to those of the previous one as explained above.

In Fig. 2, we presnt the calculated electron energy bands of ZnSe from calculation III (solid lines) and calculation IV (dashed lines). Here $\Gamma = (0,0,0)$; $L = (1,1,1)\pi/a$; $X = (0,1,0)2\pi/a$; $K = (3/4,3/4,0)2\pi/a$.[35] The zero of the energy was set at the top of the valence bands. The calculated energies of the occupied valence bands and the unoccupied conduction bands converged to an average difference of several meV. The fourth calculation (the dashed line) of Fig. 2 gives sufficiently converged electron energy bands of ZnSe with respect to the size of the basis set. As we present in the following sections, the calculated electronic properties of ZnSe from calculation IV agree well with experimental data.

However, as we added more atomic orbitals in the calculations, the calculated electron energy bands of ZnSe drifted away from the converged results of calculation IV around the Γ-point. One may observe a computational behavior that is similar to that of the calculations for hydrogen atom. Fig. 3 shows the comparison of results from calculation IV (solid lines) and from calculation V (dashed lines). The calculated occupied energy levels converged with respect to the size of the basis set. However, some of the calculated unoccupied energy levels become lower than those of the calculation IV, as more atomic orbitals are added in the calculations. Different from the case of hydrogen atom, there was no an exact solution for the electronic structure of ZnSe as a reference. Various physical interpretations were devised to explain the numerical performance of the Ritz-process in the calculations. Some of them were believed to contribute in various aspects to the problem. In fact, the problem was previously claimed as the failure of density functional theory or the failure of local density functional calculations in many occasions. Part of the support for this claim was due to the fact that the calculated conduction band energies (or the band-gap energies) of semiconductors utilizing various computational methods often

of states (DOS) of ZnSe in Fig. 4, as obtained from calculation IV. The total DOS curve in Fig. 4, particularly the inset, indicates that the small values of the density of states from 2.6 eV to 2.9 eV strongly suggest that measurements or related analysis that are not very sensitive may not detect the smallest energy gap.

Our calculated effective mass of n-type carriers, m_n^*, near the Γ-point is 0.15 m_0, where m_0 is the free-electron mass. This result is in good agreement with the experimental value of $0.16m_0$.[40, 39] The calculated effective mass of n-type carriers, away from the Γ-point, is between $0.15m_0$ and $0.17m_0$.

We also performed the self-consistent ab-initio calculations for the electronic structure of ZnSe, utilizing local density approximation for the exchange-correlation potential. We compared the electron energy bands from the LDA and GGA calculations. The average difference between the resulted bands of the two calculations is of the order of 1 mRy.

3.3 Electronic Structure of Ge

We performed the self-consistent ab-initio calculations for the electronic structure of crystalline Ge in the diamond structure. We used a zero temperature lattice constant of $a = 5.63\mathring{A}$ in these calculations.[39] We tested the convergency of the electronic structure calculation with respect to the size of the basis sets of atomic orbitals. We calculated the atomic wave function using a separate computer program that employed ab-initio density functional computations for atoms. We expanded the atomic wave functions as a linear combination of Gaussian orbitals (LCGO) in real space as discussed in the previous section.

In the calculation of the electronic structure of Ge, we employed non-local density functional potentials in the generalized gradient approximation that was developed by Perdew and Wang.[22] We first carried out completely self-consistent calculations for crystalline Ge using a basis set that included atomic orbitals of Ge(1s2s3s4s 2p3p4p 3d). We then repeated the self-consistent calculation using an augmented basis set that also included the orbital of Ge($4d^0$). In the self-consistent calculations of the electronic structure of solid Ge, we considered Ge(1s2s 2p) as the core states. All other states were treated as valence states and were allowed to relax in the self-consistent calculations. We then plotted the resulting energy bands from these two distinct self-consistent calculations. We observed that the occupied and unoccupied bands from the two calculations differ considerably.

The next step was to repeat our procedure for the third, fourth, and

3.4 Electronic Structure of GaAs

We also applied the same calculation procedure as discussed in the previous sections to the study of the electronic structure of GaAs in the zinc blende structure. We used the experimental lattice constant of $a = 5.65\mathring{A}$ in the calculations.[43, 44] We calculated the atomic wave functions of Ga and As self-consistently. We evaluated the charge transfer in GaAs from the self-consistent ab-initio calculations of the electronic structure. Ga atoms in GaAs lose about 0.3 to 0.4 electrons per atom to As atoms. In the self-consistent ab-initio calculations, we employed non-local density functional potentials in the generalized gradient approximation. We used the 1s, 2s, and 2p states of Ga and As as the core states in the frozen core approximation, and allowed all other states to relax in the self-consistent ab-initio calculations. In Fig. 6, we present the calculated electron energy bands of GaAs along some high symmetry directions in the Brillouin zone. Here $\Gamma = (0,0,0)$; $L = (1,1,1)\pi/a$; $X = (0,1,0)2\pi/a$; $K = (3/4,3/4,0)2\pi/a$. The zero of the energy was set at the top of the valence bands. In Fig. 6, the solid lines represent the calculated results using the atomic orbitals of Ga(1s2s3s4s 2p3p4p 3d4d) and As(1s2s3s4s 2p3p4p 3d4d), where Ga(4d) and As(4d) are the unoccupied atomic orbitals. The dashed lines represent the calculated bands for the basis set that has an additional atomic orbital of As(5s). The calculated electron energy bands of the occupied states of GaAs from the two different calculations agree very well. The average difference of the energies of the occupied states from these two calculations is about several meV.

GaAs has a direct band-gap at the Γ-point as shown in Fig. 6. The lowest energy state of the conduction band is at the Γ-point. The lowest energy of the conduction band at the L-point is higher than that at the Γ-point by 0.2 eV. This result agrees well with the experimental value of 0.2 to 0.3 eV.[44] The theoretical band-gap energy of GaAs is 1.24 eV from this calculation. The reported experimental values of the band-gap energy of GaAs is 1.4 to 1.5 eV.[43, 44, 45] As we discussed in the previous sections, we present below the calculated electron density of states of GaAs in Fig. 7. There is a tail structure near the conduction band edge. The small values of the density of states from 1.24 eV to 1.7 eV strongly suggest that measurements or related analyses that are not very sensitive may not detect the smallest energy gap.

We also calculated the effective mass m^* of the electrons (n-type carriers) in the lowest conduction band near the Γ-point. The effective mass m^* is calculated from the curvature of the band dispersions. The calculated

[2] W. Kohn and L. J. Sham, Phys. Rev. **140**, A1133 (1965).

[3] J. Callaway and N. H. March, *Solid State Physics*, **38**, edited by H. Ehrenreich, D. Turnbull, and F. Seitz, (Academic Press, New York, 1984), p135, and references therein.

[4] M. L. Cohen, Science, **261**, 307 (1993).

[5] W. Y. Ching, J. Amer. Ceramic Soc. **73**, 3135 (1990).

[6] *Theory of the Inhomogeneous Electron Gas* 1983, edited by S. Lundqvist and N. H. March (Plenum, New York), and references therein.

[7] *Electronic Structure, Dynamics, and Quantum Structural Properties of Condensed Matter* 1985, edited by J. T. Devreese and P. van Camp, vol. 121 of NATO Advanced Study Institute. Series B: Physics (Plenum, New York), and references therein.

[8] G. B. Bachelet and N. E. Christensen, Phys. Rev. B **31**, 879 (1985).

[9] M. Rohlfing, P. Krüger and J. Pollmann, Phys. Rev. B **48**, 17791 (1993).

[10] L. J. Sham and M. Schlüter, Phys. Rev. Lett. **51**, 1418 (1985); Phys. Rev. B **32**, 3883 (1985).

[11] J. P. Perdew and M. Levy, Phys. Rev. Lett. **51**, 1884 (1985).

[12] M. S. Hybertsen and S. G. Louie, Phys. Rev. Lett. **55**, 1418 (1985); Phys. Rev. B **34**, 5390 (1986).

[13] X. Zhu and S. G. Louie, Phys. Rev. Lett. **56**, 2415 (1986).

[14] M. Rohlfing, P. Krüger and J. Pollmann, Phys. Rev. B **48**, 17791 (1993).

[15] O. Zakharov, A. Rubio, X. Blase, M. L. Cohen, and S. G. Louie, Phys. Rev. B **50**, 10780 (1993).

[16] M. Oshikiri and F. Aryasetiawan, Phys. Rev. B **60**, 10754 (1999).

[17] F. Aryasetiawan and O. Gunnarsson, Rep. Prog. Phys. **61**, 237 (1998).

[18] K. A. Johnson and N. W.Ashcroft, Phys. Rev. B **58**, 15548 (1998).

[19] M. Städele, M. Moukara, J. A. Majewski, P. Vogl, and A. Görling, Phys. Rev. B **59**, 10031 (1999).

[36] E. L. Briggs, D. J. Sullivan, and J. Bernholc Phys. Rev. B **52**, R5471 (1995).

[37] T. L. Chu, S. S. Chu, G. Chen, J. Britt, C. Ferekides, and C. Q. Wu, J. Appl. Phys. **71**, 3865 (1992).

[38] J. Z. Zheng and J. W. Allen, Phys. Rev.B. **49**, 7770 (1994).

[39] Landolt-Börnstein New Series III, vol. 22a, *Zahlenwerte und Funktionen aus Naturwissenschaften und Technik*, edited by O. Madelung, (Springer, New York, 1987).

[40] P. J. DEAN, D. C. HERBERT, A. M. LAKEE, Proc. 15th Int. Conf. Physics of Semiconductors , Kyoto, J. Phys. Soc. Jpn. **49**, Suppl. A, 185 (1980).

[41] S. H. Gould, *"Variational Methods for Eigenvalue Problems"*, (University of Toronto Press, 1957), ch. 2.

[42] D. Bagayoko, Inter. J. of Quantum Chemistry **17**, 527 (1983).

[43] S. Adachi, J. Appl. Phys. **58**, R1-R29 (1985).

[44] Landolt-Börnstein New Series III, vol. 17a, *Zahlenwerte und Funktionen aus Naturwissenschaften und Technik*, edited by K. H. Hellwege and O. Madelung, (Springer, Berlin, 1982).

[45] A. R. Goni, A. Cantarero, K. Syassen, and M. Cardona, Phys. Rev. B **41**, 10111 (1990).

Table 2: Calculated electronic energies (eV) of Ge at the selected high symmetry points. The experimental data are from Reference [39, 44].

Ge	Calculation	Deg	Measurements
Γ_{1v}	-12.59	1	-12.6, -12.9±0.2
Γ'_{25v}	0.0	3	0.0
Γ'_{2c}	0.83	1	0.89
Γ_{15c}	2.81	3	3.01
L'_{2v}	-10.41	1	-10.6±0.5
L_{1v}	-7.44	1	-7.7±0.2
L'_{3v}	-1.39	2	-1.4±0.3
L_{1c}	0.62	1	0.74
L_{3c}	4.02	2	4.3±0.2, 4.2±0.1
L'_{2c}	8.29	1	7.8±0.6, 7.9±0.1
X_{1v}	-8.64	2	-9.3±0.2
X_{4v}	-3.00	2	-3.15±0.2, -3.5±0.2
X_{1c}	1.04	2	1.3±0.2
X_{3c}	9.98	2	
E_g	0.62		0.66, 0.74

Table 3: The effective masses (in m_0) of the n-type carriers at the lowest conduction band of Ge in the diamond structure.

	calculation	measurements
$m_{n\perp}(L_{1c})$	0.086	0.0807[39]
$m_{n\parallel}(L_{1c})$	1.43	1.57[39]
$m_{n\Gamma}$	0.043	0.038[39]

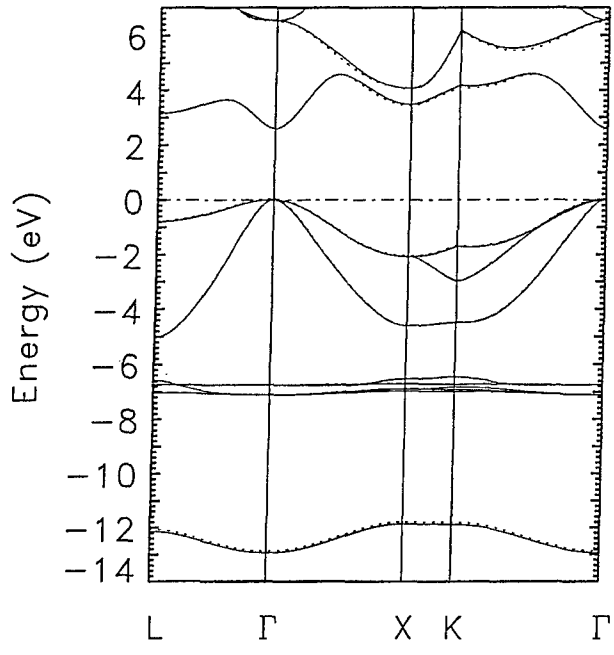

Figure 2: The calculated electronic energy bands of ZnSe along the high symmetry directions. The solid and dashed lines represent the results of calculations III and IV, respectively.

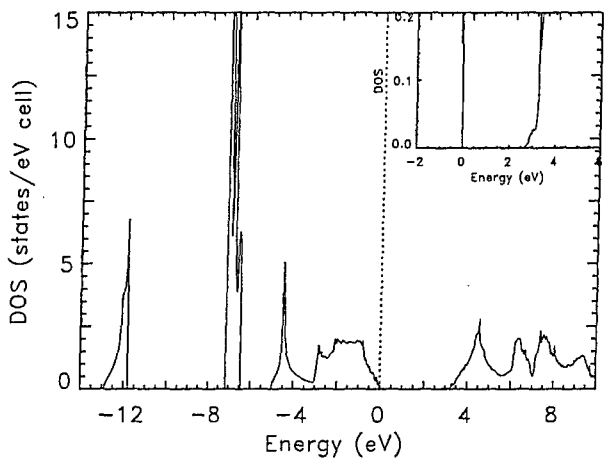

Figure 4: The calculated density of states of ZnSe. The inset shows the tail structure of the density of states of ZnSe near the bottom of the conduction bands.

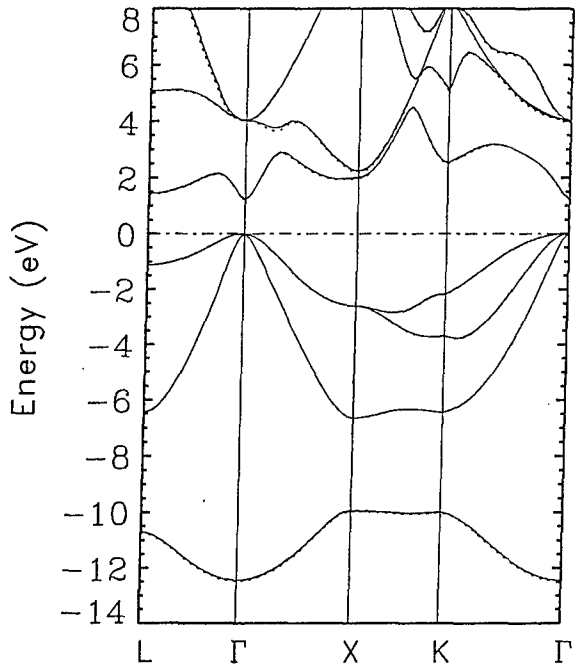

Figure 6: The calculated electron energy bands of GaAs.